Pacific modulation of accelerated south Indian Ocean sea level rise during the early 21st Century

J. Jyoti[1,2] · P. Swapna[1] · R. Krishnan[1] · C. V. Naidu[2]

Abstract

The south Indian Ocean has shown an unprecedented sea-level rise during the early 21st Century. Sea-level rise in the south Indian Ocean is found to be 37% quicker than the global mean sea-level during 2000–2015. Observational datasets and long-term proxy records identify Pacific origin of the south Indian Ocean sea-level rise. Our results indicate that co-evolution of the cold phase of Pacific decadal oscillation (PDO) and prolonged La Niña-like condition enhances the equatorial Pacific easterlies. Stronger in-phase association of these major Pacific climate modes and equatorial Pacific easterlies enhances the Indonesian throughflow (ITF), transporting fresh and warm water anomalies from western tropical Pacific into the south Indian Ocean. As a result, south Indian Ocean sea-level rise has accelerated more than the global, with 40% contribution from the halosteric sea level primarily through the ITF transport and a secondary from the local processes during 2000–2015. The co-evolution of PDO and the south Indian Ocean sea level is also evident from the long-term proxy records indicating that the association is part of an internal mode of variability modulated on decadal time-scales. The finding from the study cautions that accelerated heat and freshwater intrusion from the western Pacific with the co-evolution of PDO and La Niña-like condition may lead to the accelerated sea-level rise and marine heat waves in the south Indian Ocean imposing threats to the life of coral reefs and marine ecosystems.

Keywords South Indian Ocean sea-level rise · Pacific decadal oscillation · La Niña · Indonesian Throughflow · Marine ecosystem

1 Introduction

The Oceans have absorbed about 93% of the excess heat due to anthropogenic global warming during the past half-century (Rhein et al. 2013). The excess heat and melting of continental ice sheets have contributed to the global mean sea-level rise of about 3.3 ± 0.5 mm year^{-1} during 1993–2015 (Chen et al. 2017; Legeais et al. 2018; Nerem et al. 2018). However, sea-level rise is not globally uniform

✉ P. Swapna
  swapna@tropmet.res.in

1 Centre for Climate Change Research, Indian Institute of Tropical Meteorology, Pune 411008, India

2 Department of Meteorology and Oceanography, College of Science and Technology, Andhra University, Vishakhapatnam 530003, India

(Bindoff et al. 2007; Woodworth and Player 2003), sea-level variability, as well as trends, differs from region to region. The Indian Ocean sea level has shown a distinct spatial pattern with a substantial increase in the north (Han et al. 2010; Srinivasu et al. 2017; Swapna et al. 2017; Thompson et al. 2016) and south of 20°S (Fig. 1a, b). Sea-level rise in the north Indian Ocean is 3.3 mm year^{-1} during 1993–2015, similar to the global mean sea-level rise (Swapna et al. 2017). Interestingly, the south Indian Ocean has shown an accelerated sea-level rise of about 5.2 mm year^{-1} that is 37% quicker than the global mean sea-level rise during 2000–2015 (Fig. 1c). However, the contributing factors for the accelerated sea-level rise in the south Indian Ocean are poorly described and understood.

South Indian Ocean has received considerable attention with the identification of global warming "hiatus" (England et al. 2014; Meehl et al. 2011). Moreover, the transport of the heat from the western Pacific into the south Indian Ocean during the hiatus period was identified as the dominant mechanism for the slowdown of global warming temperature
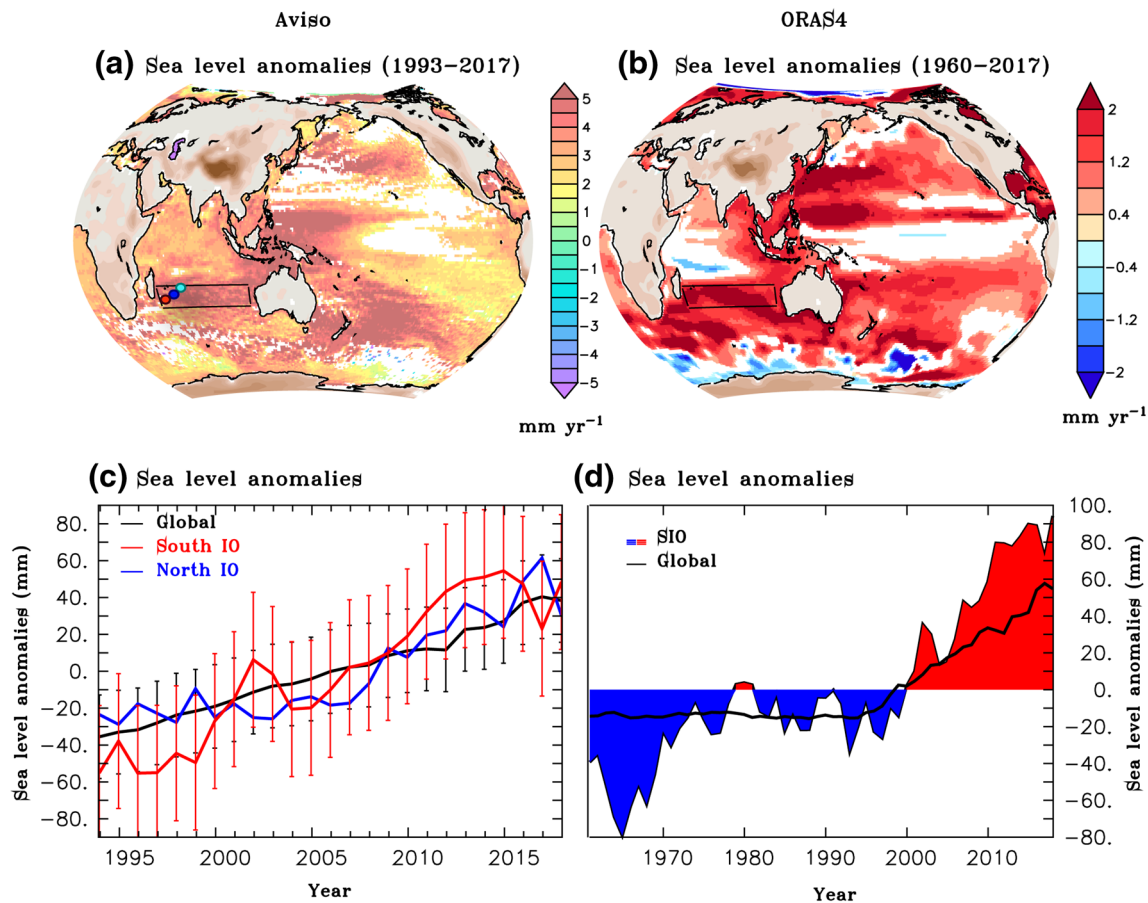
Fig. 1 The spatial map of Man-Kandall trend of sea-level anamolies (mm year⁻¹) from **a** Aviso (1993–2017), and **b** ORAS4 (1960–2017). The regions at a 90% significance level are shaded. Time series of annual mean sea-level anomalies (mm) from **c** Aviso averaged over the north Indian Ocean (blue curve; 50°E–110°E, 5°S–25°N), south Indian Ocean (red curve; 50°E–110°E, 20°S–30°S) and global mean (black curve); the error bars are based on one standard deviation are shown for the global and south Indian Ocean mean sea level with respective colors, **d** ORAS4 averaged over the south Indian Ocean (shaded curve) and global mean (black curve). The study region (50°E–110°E, 20°S–30°S) is highlighted by a rectangle in **a**, and **b**

(Dong and McPhaden 2016; Lee et al. 2015; Liu et al. 2016). In addition to modulating global temperature, excess heat transport has resulted in increasing intensity of marine heat waves (Oliver et al. 2018) in the south Indian Ocean causing widespread mass coral bleaching events, threatening the integrity and functional diversity of coral reefs (Zinke et al. 2015; Feng et al. 2015a). Concomitantly, the south Indian Ocean also has shown an accelerated sea-level rise. It has been observed that the south Indian Ocean sea-level rise is much higher than the global mean sea level during the same period (Fig. 1). It remains unclear whether the enhanced sea-level rise in the south Indian Ocean is forced solely by the heat transport from the Pacific, hence we aim to clarify the possible contributing factors for such an accelerated sea-level rise in the south Indian Ocean.

Recently, many studies have demonstrated the role of Indonesian Throughflow (ITF) into the Indian Ocean, driven by enhanced trades associated with the negative phase of Pacific decadal oscillation (PDO), in regulating the heat budget during the recent hiatus (Lee et al. 2015; Nieves et al. 2015). More recently, a study by Dong and McPhaden (2016) also identified a remote influence of the Pacific through increase ITF in the Indian Ocean. While Li et al. (2017) have shown that strengthening of the Pacific trade winds and the ITF associated with the negative phase of the interdecadal Pacific oscillation (IPO) has resulted in the warming of the southeast Indian Ocean by the enhanced heat transport from the western Pacific into the south Indian Ocean. The heat transport mechanism and warming in the southeast Indian Ocean have been discussed by many of the recent studies (Li et al. 2018; Zhang et al. 2018). The study by Llovel and Lee (2015) discussed the sea-level rise in the south Indian Ocean during 2005–2015 forced by the freshwater transport resulting from the enhanced precipitation over the maritime continent region, with additional contribution from the western tropical Pacific. While Feng et al.

(2015b) have reported the existence of freshwater anomalies in the ITF. However, it is intriguing to note that sea-level rise in the south Indian Ocean has been accelerating since 2000, but maritime continent precipitation might have any significant role prior to this period. Most of the previous studies either discussed the tropical south Indian Ocean sea-level rise driven by wind-driven linear ocean dynamics associated with local and remote contributions (Schwarzkopf and Boning 2011; Nidheesh et al. 2013; Trenary and Han 2013; Han et al. 2014; Li and Han 2015; Qu et al. 2019) or heat contribution from the western Pacific to the south Indian Ocean. Therefore, the sea-level rise in the south Indian Ocean, which is much higher than the global mean needs a better understanding of the large-scale forcing as well detailed analysis of various contributors to the mean sea-level through a sea-level budget analysis, which has been lacking in the Indian Ocean.

Sea-level budget analysis can provide more insight into the contributors to sea-level rise. Several previous studies have addressed the global sea-level budget over different time-scales using different datasets (Chambers et al. 2017; Dieng et al. 2017; Dong and Zhou 2013; Landerer et al. 2007; WCRP Global Sea Level Budget Group 2018). The global mean sea-level is a combination of ocean volume change associated with thermal expansion (thermosteric), salinity changes (halosteric) and change in the mass of the ocean due to the melting of continental ice and filling of continental reservoirs (eustatic). The global sea-level budget estimates indicate that global mean steric trends contributed to 1.38 ± 0.16 mm year^{-1} compared with a total trend of 2.74 ± 0.58 mm year^{-1} during the period 2002–2014 (Rietbroek et al. 2016). However, estimation of a regional sea-level budget is complicated, the dominant components of regional sea-level budget exhibit large regional variability (Rietbroek et al. 2016). Regionally, sea level can be altered by long-term changes in wind stress, atmospheric pressure, and changes in heat and freshwater fluxes at the ocean surface and boundaries (Dangendorf et al. 2014). For example, the north Indian Ocean sea-level rise is dominated by the thermosteric changes (Thompson et al. 2016) and is mainly driven by the changes in the summer monsoon circulation (Swapna et al. 2017). Therefore, understanding the accelerated sea-level rise in the south Indian Ocean demands a detailed sea-level budget analysis, which has not been explored before.

This study presents regional sea-level budget analysis and identifies dominant contributors to the accelerated sea-level rise in the south Indian Ocean during the recent global warming hiatus period. The novelty of the work is that we are establishing for the first time, the significant role of freshwater intrusion from the western Pacific in rising the sea level in the south Indian Ocean during the recent global warming hiatus. The study highlights the role of the western Pacific in modulating both temperature and salinity in the south Indian Ocean and thus the sea-level rise, along with a contribution from the local processes. Additionally, for the first time, we are presenting Pacific teleconnection to the south Indian Ocean sea level using proxy records. We also address whether the south Indian Ocean sea-level variability is part of an internal mode of variability modulated on decadal time-scales. The remaining paper is structured as follows. Section 2 describes observational, reanalysis, proxy datasets, and methodology used in the study. Section 3 presents the regional sea-level budget in the south Indian Ocean and the mechanism for the enhanced sea-level rise. Long-term coral records revealing the role of the internal mode of variability to the southern Indian Ocean sea level are discussed in Sect. 4. Summary and conclusion are presented in Sect. 5.

2 Data sets and methodology

2.1 Observations and proxy records

Prior to 1993, sea-level rise estimates relied on the tide gauge measurements. Here, we use available long-term (more than 30 years) tide gauge records in the south Indian Ocean, obtained from the archives of Permanent Service for Mean Sea Level (PSMSL; Woodworth and Player 2003). The Satellite-derived sea-level anomaly from the Archiving, Validation, and Interpretation of Satellite Oceanographic (Aviso; Ducet et al. 2000) cover the period January 1993–December 2017. This sea-level dataset is based on TOPEX/Poseidon, Jason-1 and Jason-2 for the global domain.

To quantify the steric sea-level (SSL) variations resulting from temperature and salinity, we have considered different reanalysis and gridded Argo datasets. These datasets are as follows.

ORAS4 (Balmaseda et al. 2013) available as monthly temperature, salinity and sea surface height field for the period of 1958–2017, Ishii et al. (2017) updated version 7.2 for the period of 1955–2017, EN4 (Good et al. 2013) version 4.2.0 available for 1900–2017, high resolution (0.25×0.25) ECCO2 reanalysis (Menemenlis et al. 2008) for the period of 1992–2018, and NOAA (Levitus et al. 2012). The NOAA data are available as yearly and 5-year running means SSL anomalies from the surface to 2000 m depth during 1950–2016. Additionally, the Ocean surface currents from ORAS4 for the same period have been utilized.

After 2005, sufficient Argo floats are available to compute SSL anomalies. For this study, we utilize three different gridded Argo products of temperature and salinity down to 2000 m depth at monthly intervals. They are the Japan Agency for Marine-Earth Science and Technology

(JAMSTEC; Hosoda et al. 2008), CSIO (BOA), and the International Pacific Research Centre (IPRC). The precipitation from the Global Precipitation Climatology Project (GPCP; Adler et al. 2003) and evaporation from Era-interim (Berrisford et al. 2009) during 1979–2017, Met Office Hadley Centre Sea-level Pressure (HadSLP2; Allan and Ansell 2006) and surface winds from the National Centres for Environmental Prediction (NCEP; Kistler et al. 2001) during 1950–2017 are used. Additionally, the surface wind product from ERA-Interim (Berrisford et al. 2009), Quickscat (Fore et al. 2014) during 1979–2017 and 1999–2009, respectively, and Tropflux wind stress and net surface heat flux (Praveen Kumar et al. 2012) during 1979–2017 has been utilized. Additionally, we use monthly outputs of net surface heat flux from the objectively analyzed air-sea fluxes (OAFlux; Yu et al. 2008), NCEP and ERA-interim. Different climate mode indices used are; the Pacific decadal oscillation (PDO, http://www.esrl.noaa.gov/psd/data/correlation/pdo.data), interdecadal Pacific oscillation (IPO, https://www.esrl.noaa.gov/psd/data/timseries/IPOTPI/tpi.timseries.ersstv5.filt.data), and Oceanic Niño (ONI, https://www.esrl.noaa.gov/psd/data/correlation/oni.data) Index.

The proxy records of sea-level reconstruction during 1795–2010 derived from Houtman Abrolhos Island Sr/Ca, Oxygen Isotopes (Zinke et al. 2015) and PDO reconstruction based on Ogasawara Coral Winter Sr/Ca and U/Ca for the period of 1873–1994 (Felis et al. 2010). The mean annual cycle is removed by subtracting the climatological mean for each month. The analyses presented in the study are based on annual mean quantities.

2.2 Methodology and standard equations

Steric sea level and components: The steric, thermosteric and halosteric sea level are computed over the upper 2000 m of the ocean following standard methods, such as detailed in Swapna et al. (2017)

$$\eta^{thermosteric}(\tau) = \eta(\tau^r) - \frac{1}{\rho_0} \sum dz \lfloor \rho(\theta, S^r, p^r) - \rho(\theta^r, S^r, p^r) \rfloor$$

$$\eta^{steric}(\tau) = \eta(\tau^r) - \frac{1}{\rho_0} \sum dz \lfloor \rho(\theta, S, p^r) - \rho(\theta^r, S^r, p^r) \rfloor \quad (1)$$

$$\eta^{halosteric}(\tau) = \eta(\tau^r) - \frac{1}{\rho_0} \sum dz \lfloor \rho(\theta^r, S, p^r) - \rho(\theta^r, S^r, p^r) \rfloor,$$

where, $\eta^{thermosteric}(\tau)$ is the thermosteric sea level at a time (τ), similarly $\eta^{steric}(\tau)$ and $\eta^{halosteric}(\tau)$ are steric and halosteric sea level at a time (τ). Variables with an "r" superscript refer to reference state values so that $\eta(\tau^r)$ is the sea level at the reference state, ρ_0 is a globally constant Boussinesq reference density, θ is the potential temperature of seawater, S is the salinity and p pressure. We choose the upper 2000 m

as this depth range corresponds to that with the most available observational data.

Sea-level budget equation: The mean sea-level change is a function of time t and is usually expressed by the sea-level budget equation as below

$$MSL(t) = MSL(t)_{steric} + MSL(t)_{mass} + R_S, \quad (2)$$

where MSL (t) is the total sea level, MSL (t)$_{steric}$ is the steric component of sea level in the upper 2000 m, and MSL (t)$_{mass}$ is the ocean mass component of sea level. The residual is expressed as R_S. The residual may be due to the mass added through the Throughflow.

Ekman transport: The estimates of meridional Ekman transport (M_{Ek}) which is primarily contributed by the zonal component of wind stress which is estimated by following standard method detailed in Sprintall and Liu (2005)

$$M_{Ek} = -\frac{1}{f \rho_0} \int_{x_w}^{x_e} \tau^x dx, \quad (3)$$

where τ^x is the zonal wind stress, ρ_0 is the average water density over the upper layer (assumed constant at 1025 kg m^{-3}), and f is the Coriolis parameter, x_e and x_w are the locations of eastern and western boundaries, respectively. x_e is 115°E and x_w is 131°E in the analysis.

Similarly, the thermosteric and halosteric components of ITF transport are estimated following the method by Hu and Sprintall (2017)

$$Q_\lambda = \frac{gH^2 \Delta_\rho}{2f_\lambda \rho_0},$$

$$ITF = Q_{\lambda_N} - Q_{\lambda_S}, \quad (4)$$

where g is gravity acceleration, f_λ is the Coriolis parameter at latitude λ, H is the penetration depth that approximately equals the sill depth of ITF (set to be 1200 m), ρ_0 is the reference density at 1200 m, and Δ_ρ is the density difference between the (9°S–15°S, 100°E–120°E), where the ITF exits into the Indian Ocean, and (6°S–6°N, 80°E–100°E) the region of denser water in the eastern equatorial Indian Ocean. $\lambda_N = 10°S$ (Northern), and $\lambda_S = 16°S$ (Sothern) boundary latitudes. The thermal and halosteric ITF transport are, respectively defined as ITF$_T$ = ITF (T, $\bar{S}$) and ITF$_S$ = ITF ($\bar{T}$, S) where $\bar{T}$ and $\bar{S}$ are climatological temperature and salinity.

To quantify the relative contributions of ITF$_T$ and ITF$_S$ to ITF, we calculate the percentage of absolute values (P_i) of ITF$_T$ and ITF$_S$ relative to the total variation following the method of Hu and Sprintall (2017)

$$P_i = \frac{|ITF_i|}{|ITF_T| + |ITF_S| + |ITF_R|} \times 100\%, \quad (5)$$

where 'i' is T or S, ITF_R the residual term equals $ITF - ITF_T - ITF_S$. We have also estimated the uncertainty in SSL and SSH. The detailed methodology for the uncertainty estimates is discussed in supporting information eqn. (S1)

3 Results

3.1 Observed sea-level rise in the south Indian Ocean

The south Indian Ocean is bounded by the African coast to the west and by Sumatra, Java, and the Western Australian coast to the east and connects to the Southern Ocean to the south. It receives approximately 15 million $m^3 s^{-1}$ of water flow from the Pacific Ocean through the Indonesian seas (Gordon et al. 2010) known as ITF. The majority of ITF flows westward across the Indian Ocean in the south equatorial current (Qu et al. 2005; Zhou et al. 2008) and feeds upwelling in the thermocline ridge region of the subtropical cell and some directly flow southward along the west coast of Australia in the Leeuwin current. The interannual to decadal variations in the south Indian Ocean is mainly dominated by the variability of large-scale atmospheric circulations over the Pacific through the ITF transport (Feng et al. 2011; Schwarzkopf and Boning 2011; Wijffels and Meyers 2004).

To understand the sea-level variability in the south Indian Ocean, we estimate the spatial trend of sea-level anomalies from the Aviso and ORAS4 for the period of 1993–2017 and 1960–2017, respectively. The Mann–Kendall significance trends at a 90% confidence level (Mann 1945; Kendall 1975) are shaded in Fig. 1a, b. The spatial pattern of sea-level anomalies in the Indian Ocean from both the products shows a significant rise in the north as well as the south Indian Ocean with the unprecedented rise in the south Indian Ocean. Further, to understand the time evolution of mean sea-level anomalies we averaged satellite-derived annual mean anomalies (Fig. 1c) over the global, north (50°E–110°E; 5°S–25°N) and south Indian Ocean (50°E–110°E; 20°S–30°S). This reveals an accelerated sea-level rise of about 5.2 mm $year^{-1}$ in the south Indian Ocean, which is 37% quicker than the global mean sea-level during the satellite period. Further, long-term sea-level anomalies from ORAS4 (shaded curve; Fig. 1d) also show an accelerated sea-level rise in the south Indian Ocean since 2000, which is more than the global mean (black curve), and a similar rise is also seen in the Aviso data (Fig. 1c). Similarly, the accelerated sea-level rise in the south Indian Ocean can also be seen from the spatial trend of multiple data sets including Argo data (Fig. S1). This confirms the robustness of the south Indian Ocean sea-level rise seen in various datasets. As the sea-level rise has accelerated since 2000,

we have performed a sea-level budget analysis in the south Indian Ocean to understand the contributors to the enhanced sea-level rise.

3.2 Sea-level budget in the south Indian Ocean

As sea-level rise is highly non-uniform and exhibits large regional variation, it is important to understand major contributors to regional sea-level rise. With the availability of satellite data, great progress has been achieved in understanding individual components of the sea level at global as well as regional scales (Church and White 2011; Rhein et al. 2013). It has been observed that various contributions to the sea level vary from region to region and they also differ significantly compared to the global mean sea level. It is very likely that the regional sea level is dominated by steric component while the global sea level is mostly due to water mass added to the oceans (Bindoff et al. 2007). To help quantify the dominant contributors to the sea-level rise in the south Indian Ocean, we assess the sea-level budget from ORAS4 since it provides means sea level, temperature, and salinity profiles. Additionally, we have also used observational datasets, i.e., Argo data to assess the steric component of sea level and Aviso sea level for the available period to understand the sea-level budget based on observations. The sea-level budget is performed by following Eq. (2) with SSL computed for upper 2000 m and the results are presented with an error bar of one standard deviation.

The various contributors to the budget of sea-level change in the south Indian Ocean from ORAS4 are shown in Fig. 2a. Time-series of mean sea-level (black curve) anomalies in the south Indian Ocean closely follow the SSL (red curve; Fig. 2a). The difference between mean sea level and SSL anomalies is found to be small, but not negligible (Fig. 2a; yellow dash curve). The residual may be due to the mass added through the Throughflow. This indicates that the sea-level rise in the south Indian Ocean is dominated by the SSL, which is a combination of thermosteric and halosteric components. Further, the time series of sea level and SSL show an acceleration since 2000 along with the acceleration of both thermosteric and halosteric components (Fig. 2a). This instigates us to verify possible contributions from thermosteric and halosteric components for the long-term period 1960–2015 and also for the recent period 2000–2015. Mean sea level is a combination of steric, mass and the residual. The residual term is found to be small and is considered together with the ocean mass change, expressed as the difference between mean sea level and SSL. Notably, SSL in the south Indian Ocean has the maximal contribution with 56% from thermosteric and 26% from halosteric components, respectively during 1960–2015 (Fig. 2c). Interestingly, the halosteric contribution has increased considerably (40%) during 2000–2015 (Fig. 2d).
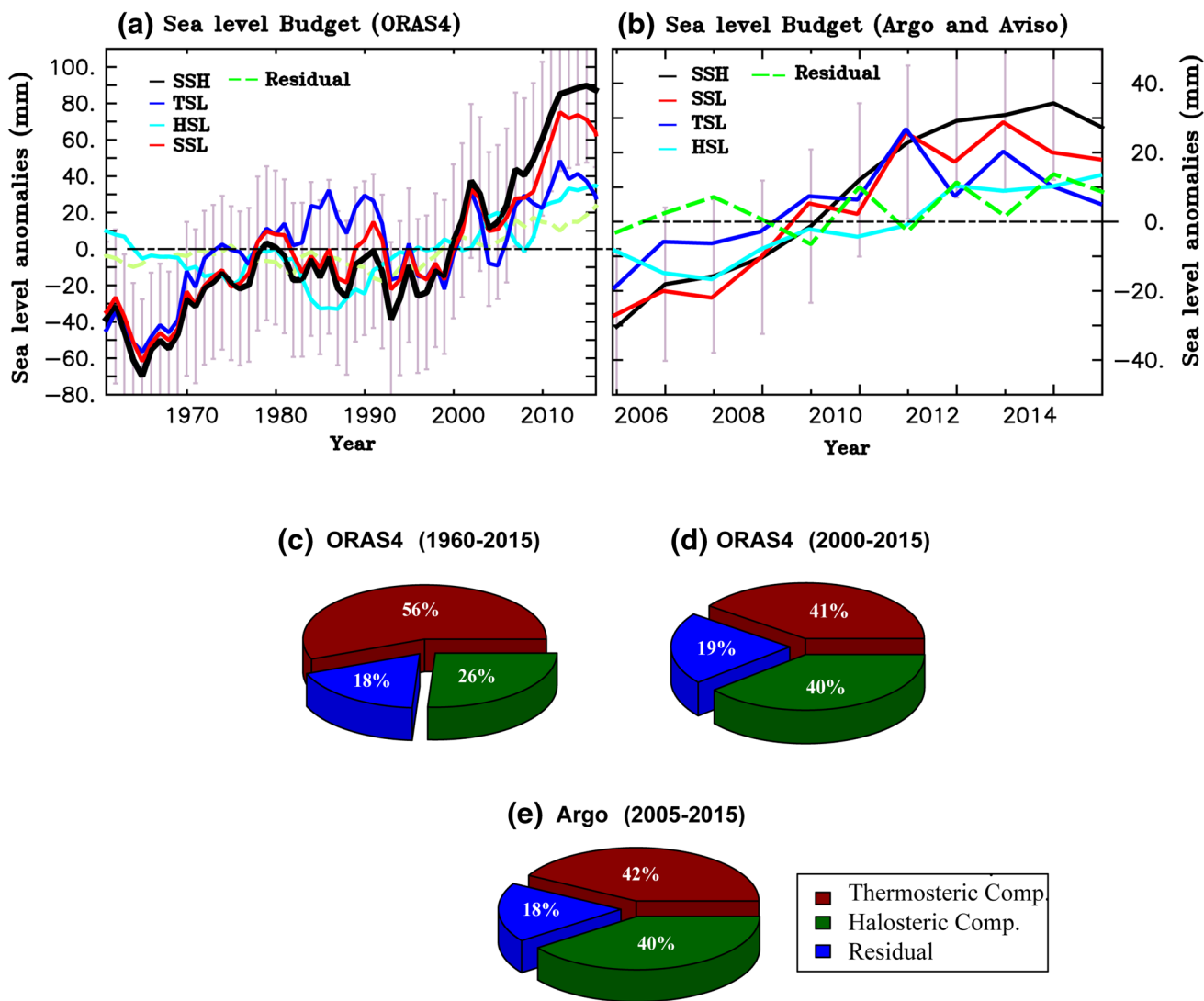
Fig. 2 Time series of components of the sea-level budget (mm) for the upper 2000 m, over the southern Indian Ocean (50°E–110°E, 20°S–30°S) from **a** reanalysis (ORAS4), **b** observations (Argo and Aviso). The error bars based on one standards deviation are shown for mean sea level. The percentage contribution of various components from **c** ORAS4 (1960–2015), **d** ORAS4 (2000–2015), and **e** Argo and Aviso (2005–2015)

We also performed the sea-level budget analysis using satellite-altimetry and Argo for better assessment using observations. Based on the common period of availability of Argo and Aviso data, the budget is performed for the period of 2005–2015 in the upper 2000 m. The Argo steric components used here are based on the ensemble mean of different Argo products mentioned in Sect. 2.1. Similar to ORAS4, the time series of SSL from the ensemble mean of Argo closely follow the mean sea-level from Aviso and thermosteric and halosteric components show an acceleration in the south Indian Ocean (Fig. 2b). The percentage contribution based on Argo and Aviso (Fig. 2e) accounts the thermosteric contribution of 42%

and halosteric contribution of 40% similar to the estimates from the ORAS4. Difference between the mean sea-level and SSL is 18% from observations (Aviso and Argo) and 19% from ORAS4 for the recent period. The acceleration of the halosteric sea-level as evident from the increased percentage contribution from both ORAS4 and observations are more than the error, indicating the robustness of the halosteric induced south Indian Ocean sea-level rise in the recent decades. This implies that an enhanced freshwater signal in the south Indian Ocean has an important role in accelerating the sea-level rise during 2000–2015. Before analyzing the source of this freshwater signal, we assess the uncertainty in the data sets used for the analysis.

3.2.1 Uncertainty analysis of steric and mean sea level

Since steric sea level is the dominant contributor to the sea-level rise in the south Indian Ocean, we briefly present the robustness of steric and mean sea level datasets used for the study. We have estimated the agreement ratio of SSL from three different reanalysis products for their common available period 1960–2015 (datasets mentioned in Sect. 2). The mathematical formulation for the estimation of agreement ratio is detailed in supporting information. Figure S2a reveals that the agreement ratio between different SSL datasets is less than one, indicating that the spread between the data sets is smaller than the amplitude of ensemble variability, thus showing better agreement between different SSL datasets. Figure S2b displays the zonal distribution of the agreement ratio averaged over the study region (20°S–30°S) in the south Indian Ocean. This ratio is less than one indicating that the spread between the products in the south Indian Ocean is very small. Since the mean

sea level data is available from ORAS4 and Aviso, we have estimated the spread between these two datasets based on the common period 1993–2015, shown in Figure S2c. The spread between Aviso and ORAS4 datasets is also less than one. Better agreement between these two data sets may be due to the fact that ORAS4 is assimilating the Aviso sea level. Further, the time evolution of sea-level anomalies from Aviso and ORAS4 with a common base period (1993–2015) is in good agreement (Fig. 3a). The accelerated sea-level rise in the recent decades, especially post-2000 can be noted from ORAS4 mean sea level (black curve), similar to the Aviso (red curve). The ORAS4 error bars are based on one standard deviation (Fig. 3a, shaded).

Time- series of steric sea level in the south Indian Ocean from ORAS4 (blue curve), Ishii (red curve), EN4 (light green curve), and NOAA (purple curve) indicate increase sea-level during last two decades and are also within the spread (Fig. 3b). The error bars in Fig. 3b are estimated based on one standard deviation (±1σ). Though
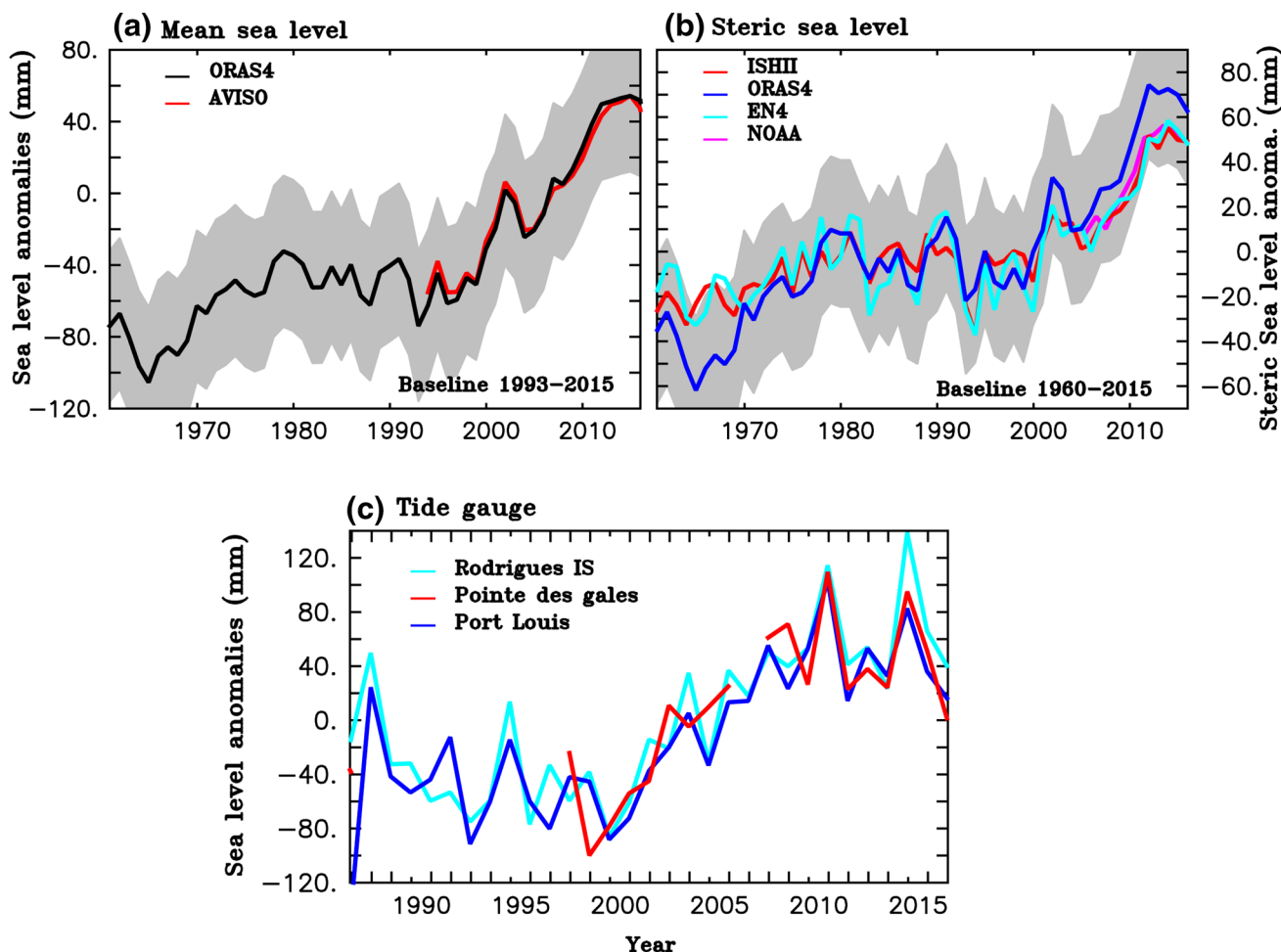

Fig. 3 Time series of annual mean anomalies (mm) in the south Indian Ocean (50°E–110°E, 20°S–30°S) of **a** mean sea level, **b** steric sea level, and **c** sea level from tide gauges. The error bars based on one standard deviation (shaded) are shown for ORAS4. The location of the tide-gauge stations marked by a circle with the same colours are shown in Fig. 1a

the SSL time-series from ORAS4 shows higher values but is within the uncertainty limit. Thus, different datasets used for the analysis are within the uncertainty limit and agrees well in the south Indian Ocean. Additionally, mean sea-level variability is dominated by SSL indicating that the sea-level rise in the south Indian Ocean is indeed dominated by the steric component.

In order to support the sea-level variability seen in the reanalysis and satellite-derived datasets, we analyze available tide gauge records namely Rodrigues Is (63.4°E, 19.6°S), Pointe des galets (55.28°E, 20.93°S) and Port Louis (57.5°E, 20.15°S) in the south Indian Ocean (Fig. 3c). The locations of the tide-gauge stations are marked in Fig. 1a. Since the data have gaps, we consider only tide gauges with a minimum of 30 years of continuous records for the most recent period. The time series of annual mean sea-level anomalies from the tide gauges in the south Indian Ocean reveals a gradual increase since 2000 similar to the reanalysis and satellite data.

3.3 Co-evolution of heat and salinity changes in the Indo-Pacific region

In this section, we investigate how the steric sea-level rise in the south Indian Ocean is associated with the changes in the Pacific. Previous studies (Han et al. 2014; Nidheesh et al. 2013; Schwarzkopf and Boning 2011; Trenary and Han 2013) have shown the role of remote Pacific variability on the south Indian Ocean. A growing body of research claims that the Pacific variability can impact the south Indian Ocean sea level through ITF, which transports heat and freshwater from the western Pacific into the south Indian Ocean (Lee and Mcphaden 2008). To help identify the Pacific contribution, we first analyze heat content and salinity anomalies in the south Indian Ocean and the Pacific Ocean.

The time-longitude Hovmoller diagram of the heat content anomalies for the upper 2000 m in the equatorial Pacific (10°S–10°N) and the south Indian Ocean (20°S–30°S) are shown in Fig. 4. The zonal wind anomalies averaged over the equatorial Pacific are contoured in Fig. 4b and the time
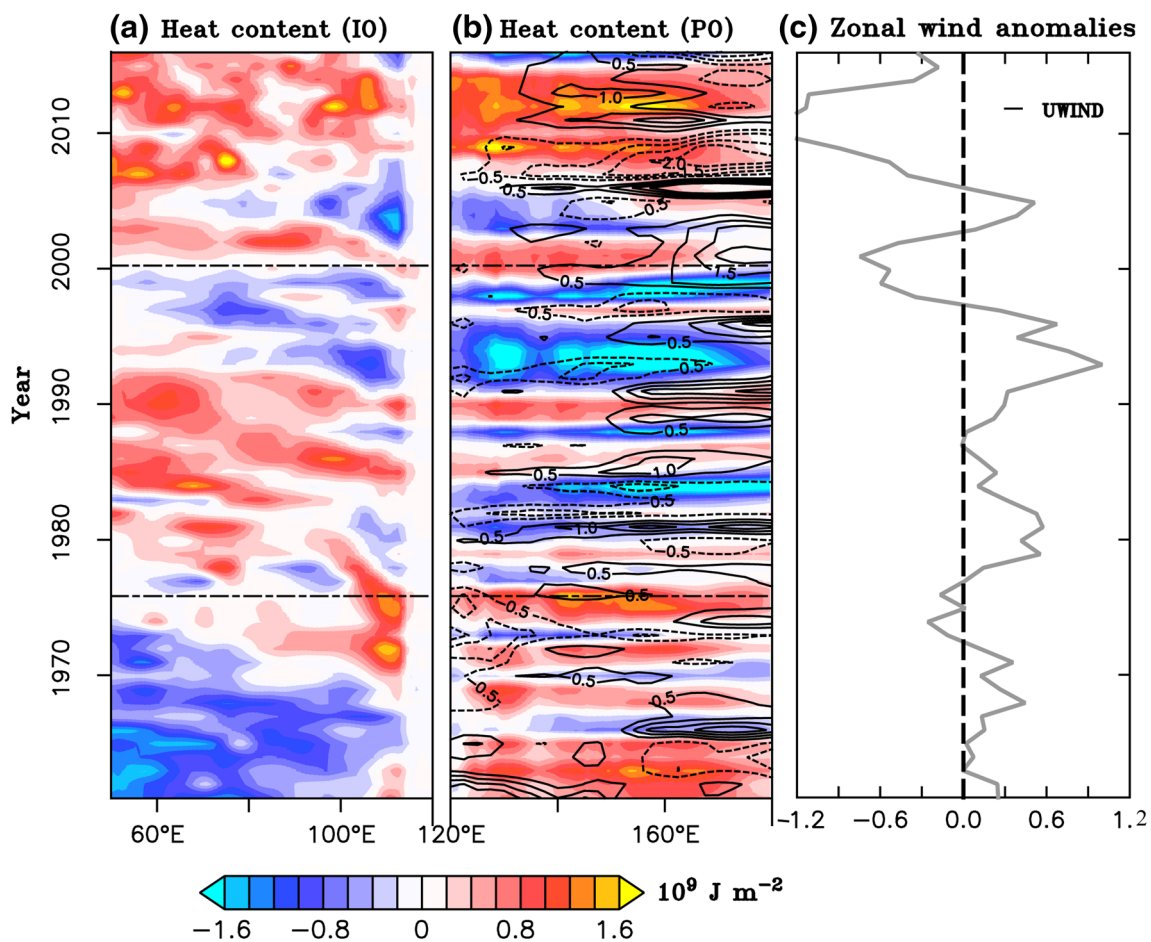

Fig. 4 The time-longitude map of heat content anomalies (shaded, 10^9 J m^{-2}) for the upper 2000 m averaged over **a** 20°S–30°S in the Indian Ocean and **b** 10°S–10°N in the Pacific. Contour in **b** are zonal wind anomalies averaged over 5°S–5°N. **c** Zonal wind anomalies averaged over western equatorial Pacific (140°E–180°E, 5°S–5°N)

evolution of zonal wind anomalies in the equatorial Pacific are also shown (Fig. 4c). We can notice the co-occurrence of heat content anomalies in the western Pacific and the southern Indian Ocean through the Indonesian seas, suggesting an oceanic connection between the Indo-Pacific regions (Fig. 4a, b). Stronger anomalous easterlies persist over the equatorial Pacific since 2000 (Fig. 4b; contours), leading to an anomalous build-up of heat and positive heat content anomalies in the western equatorial Pacific. During the same period, positive heat content anomalies are seen in the southern Indian Ocean (Fig. 4a). It can be also noted that heat content anomalies in the western Pacific were positive during 1960–1976 associated with the cold phase of PDO. During the cold phase of PDO, sea surface temperature anomalies exhibit a horseshoe pattern with warming western equatorial Pacific and vice versa during the warm phase (Mantua et al. 1997). However, equatorial Pacific easterly wind anomalies were weak (Fig. 4c, d) and thus positive heat content anomalies were not propagated in the Indian Ocean.

Apart from temperature, salinity also affects seawater density and thus sea level. Hence, it is inevitable to verify the co-evolution of salinity in the Indo-Pacific region; we

analyzed the time-longitude map of annual mean salinity anomalies for the upper 150 m (Fig. 5a, b). The annual mean salinity anomalies show anomalously high salinity water in the western Pacific and the southeastern Indian Ocean during 1960–1976 and all along the southern Indian Ocean during 1977–1999 (Fig. 5). Interestingly, these high salinity waters are replaced by anomalously low salinity water that is freshening can be seen both in the western Pacific and south Indian Ocean post-2000 period (Fig. 5a). These freshwater anomalies from western Pacific can intrude into the south Indian Ocean through oceanic pathways as discussed by Hu and Sprintall (2016). In fact, a strong linkage between the western Pacific and south Indian Ocean freshening is seen in recent decades, more details are presented in the subsequent sections.

It is also interesting to know how deep this freshwater signal can penetrate. Therefore, we analyzed a vertical profile of salinity anomalies in the south Indian Ocean (Fig. 5c). We notice that salinity anomalies in the south Indian Ocean show freshening from the surface to 150 m during the period of 2000–2015. The enhanced freshening in the south Indian Ocean in the upper 150 m is also seen
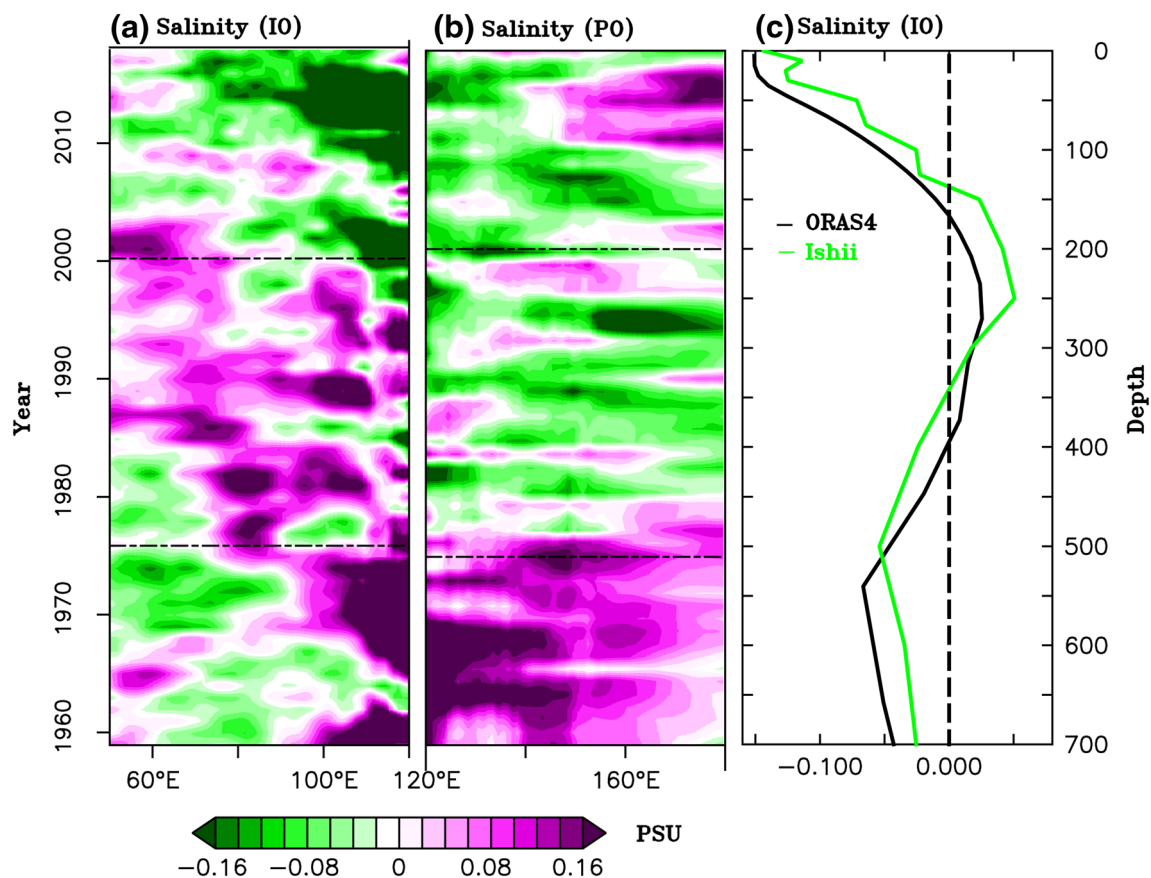

Fig. 5 The time-longitude map of salinity anomalies for the upper 150 m (shaded; PSU) averaged over **a** 20°S–30°S in the Indian Ocean and **b** 10°S–10°N in the Pacific; and **c** mean salinity (PSU) profile averaged over south Indian Ocean (50°E–110°E, 20°S–30°S)

from the salinity trends (Fig. S3) from observed and rea-nalysis datasets during 2000–2015. Thus, the co-evolution of heat and salinity anomalies in the south Indian Ocean and western Pacific implies strong association of western Pacific on the south Indian Ocean variability.

3.4 Pacific modulation to the south Indian Ocean sea-level rise

Further, to emphasize the role of the Pacific Ocean in determining the south Indian Ocean sea-level variability we analyzed dominant climate modes in the Pacific. PDO and El Niño Southern Oscillation (ENSO) (Bjerknes 1969; Mantua et al. 1997; Neelin et al. 1998; Jadhav et al. 2015) are the dominant modes of variability in the Pacific. Generally, El Niño is likely to be stronger when the PDO is in a positive phase and vice versa (Gershunov and Barnett 1998). We analyze the time-evolution of normalized (normalize with their standard deviation) PDO (red curve), ONI (black curve), IPO (light green curve) index and area-averaged zonal wind anomalies over the western equatorial Pacific (140°E–180°E, 5°S–5°N; blue curve) (Fig. 6a). A study by Han et al. (2014) has shown that IPO can be considered as a basin-wide signature of PDO and they are highly correlated (r = 0.88). Hence, we have shown the IPO index along with the PDO index and we can see that the warm/cold phases of PDO match very well with IPO. We focus on the co-evolution of PDO and ENSO and associated changes in western Pacific trade winds. A strong phase correspondence between the warm (cold) phase of PDO and ENSO with anomalous equatorial Pacific westerlies (easterlies) can be seen from Fig. 6a. During 2000–2015, when sea level (contributed from higher heat content and freshwater) was higher in the south Indian Ocean, cold phase of the PDO and prolonged La Niña-like condition persisted in the Pacific which strengthened anomalous easterlies over the western equatorial Pacific (Fig. 6a).

To further explore the contribution from enhanced heat and freshwater transport associated with strengthened easterlies over the western Pacific to the south Indian Ocean sea-level rise, we analyzed the spatial trend of SSL anomalies during 2000–2015. The SSL anomalies show a significant sea-level rise in the western equatorial Pacific and in the south Indian Ocean (Fig. 6b). The patterns of SSL trends (Fig. 6b) are consistent with those of mean sea-level trends shown in Fig. 1a. Though the Pacific forcing through ITF is important in modulating the south Indian Ocean sea level, it is also important to understand the role of local contribution. In order to understand the local vs. remote contribution, we have analyzed the various component of heat and salinity budget in the south Indian Ocean.

3.5 Local versus remote contribution to the south Indian Ocean sea level

In order to understand the contribution of ITF and local processes, analysis of different components of heat and salinity budget (detailed in supplementary section B) is performed. We analyzed the spatial trends in temperature and salinity advection (Fig. 6c, d; shaded) to understand the heat and salinity transport across the southern Indian Ocean during 2000–2015. The trend maps show anomalous horizontal advection of temperature and salinity which may be associated with heat and freshwater advection from western Pacific into the south Indian Ocean. While the trends in surface currents (Fig. 6c, d; vector) show enhancement of westward flowing south equatorial current (SEC) south of 17°S in the south Indian Ocean and is consistent with the study by Backeberg et al. (2012) who discussed the enhancement of westward SEC in response to intensified westerly winds over the south Indian Ocean. Thus, SEC helps to transport anomalously warm and freshwater water from the western tropical Pacific into the south Indian Ocean.

Though oceanic pathways through ITF is the primary contributor to the heat and salinity advection in the south Indian Ocean, the transport across other boundaries such as western boundary and Aghulas transport, and transport from the north Indian Ocean though cross-equatorial cell, may also play an important role in the heat and salinity budget in the south Indian Ocean. In the east, Leeuwin current carries warm water poleward along the west coast of Australia, driven by meridional pressure gradient set up by the ITF (Narayanasetti et al. 2016). While a large portion of the ITF transport eventually joins the Aghulas current which is primarily forced by wind stress curl in the subtropical south Indian Ocean (De Ruijter et al. 1982). In order to understand the contribution of transport across different boundaries of the south Indian Ocean and local processes, we estimated the heat and salinity advection across the boundaries following Zhang et al. (2018) (detailed in supplementary section B).

The heat and salinity advection in the upper 700 m of the control volume in the south Indian Ocean and along three cross-sections across 110°E (eastern boundary, contribution from ITF advection), 5°S (northern boundary, contribution from the cross-equatorial cell) and 30°S (southern boundary, contribution from Agulhas leakage) are estimated and are shown for the recent cold (2000–2015) minus warm (1977–1999) phase of PDO. The estimates are presented in Table 1. We can see that the heat advection across 110°E, i.e. ITF heat advection, has notable warming contribution (2.17×10^{-2} °C year^{-1}) to the south Indian Ocean heat budget. The heat advection across the southern boundary (-1.23×10^{-2} °C year^{-1}) remove heat from the south Indian Ocean and a notable decrease in heat advection is seen across the northern boundary (-0.025×10^{-2} °C year^{-1}).
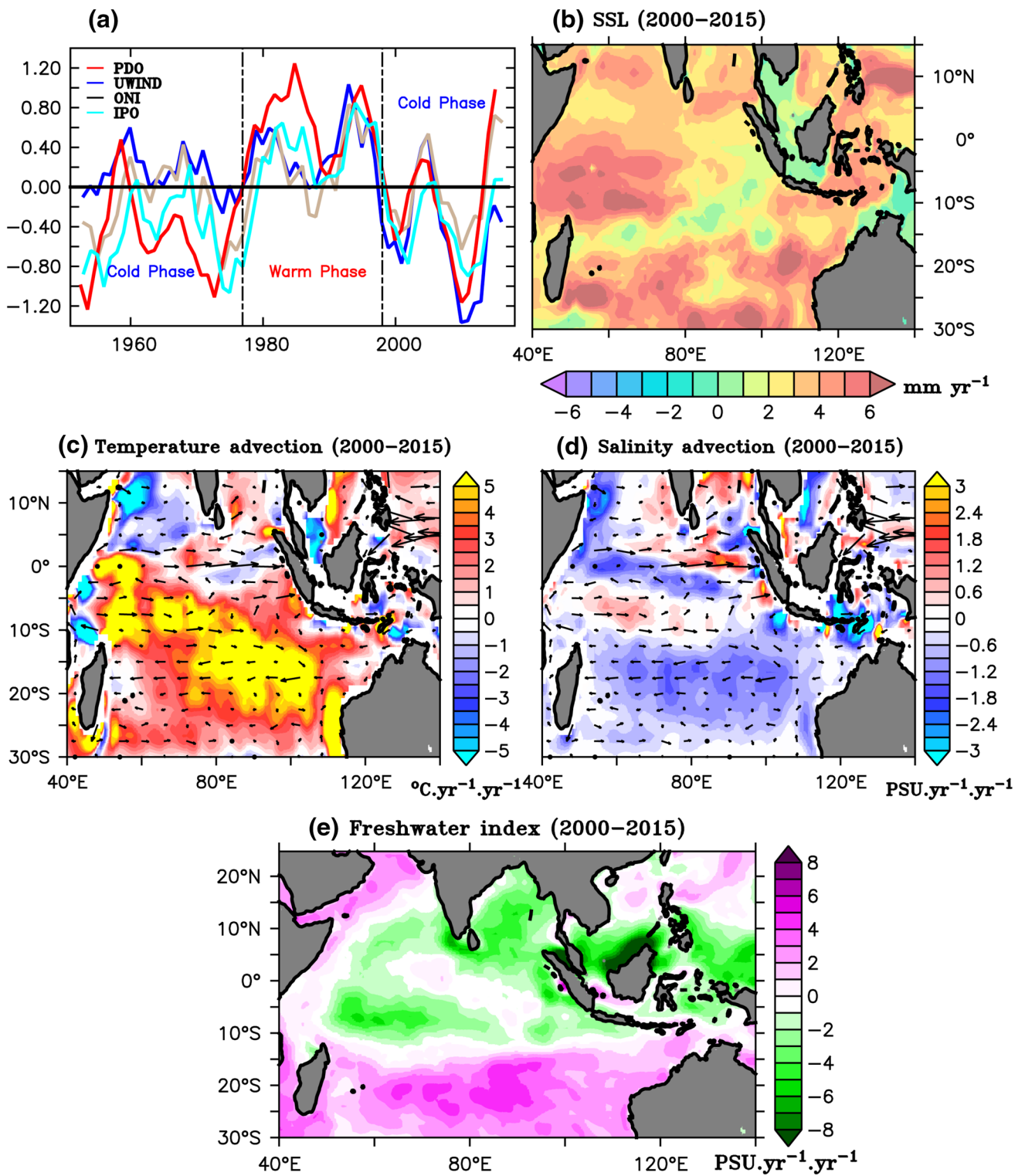
Fig. 6 Time series of annual mean **a** zonal wind anomalies (blue curve; m s^{-1}) averaged over western equatorial Pacific (140°E–180°E, 5°S–5°N), PDO (red curve), IPO (light green curve), and ONI (tan curve) index. The spatial map of annual mean trend anomalies of **b** steric sea level (mm year^{-1}), **c** temperature advec-tion (shaded; °C year^{-1} year^{-1}) and surface current [vector; (m s^{-1}) year^{-1}], **d** salinity advection (shaded; PSU year^{-1} year^{-1}) and surface current [vector, (m s^{-1}) year^{-1}], and **e** freshwater forcing (E − P, PSU year^{-1} year^{-1}) during 2000–2015

Table 1 The average difference in heat and salinity budget advective processes across individual boundaries

Cross-section	Heat advection $(10^{-2}$ °C year$^{-1})$	Salinity advection $(10^{-2}$ PSU year$^{-1})$
110°E	2.17	− 0.35[a]
5°S	− 0.025	0.27
30°S	− 1.23	− 0.14[a]

[a]Negative sign in salinity advection represents the freshwater transport

The weakening of the cross-equatorial heat transport from the north Indian Ocean in recent decades was also reported by Swapna et al. (2017). Overall the upper south Indian Ocean gains heat during the recent cold phase of PDO with primary contribution from the ITF heat advection.

We have also estimated salinity advection across the boundaries (mentioned above) of the south Indian Ocean. Similar to heat advection, the advection through ITF has a dominant (-0.35×10^{-2} PSU year^{-1}) contribution for freshwater transport into the south Indian Ocean (Table 1). We also estimated the percentage contribution of each of the terms of the budget based on eqn. S2 and eqn. S3. It can be seen that freshwater advection contributes to 66% and heat advection contributes to 55% of total salinity and heat budget in the south Indian Ocean.

We know that apart from ITF advected heat and freshwater, salinity variations can also be due to the local processes like changes in regional river runoff, local atmospheric forcing such as Ekman pumping and surface freshwater flux (evaporation minus precipitation; E − P) while local heat variation can be due to the changes in net surface heat fluxes. Since there are no major rivers discharges in the rim of the south Indian Ocean, we neglect the possible contribution from river runoff. The local contribution to freshening is evaluated by analyzing the trend in surface freshwater flux (E − P) for the same period (Fig. 6e). The trend in local freshwater forcing (E − P) in the south Indian Ocean show positive values and contributed to 21% of freshening along with Ekman pumping. The freshwater fluxes in the western Pacific show negative trends indicating that the western Pacific may be the major source of freshening in the south Indian Ocean. Similarly, contribution from local Ekman pumping (Fig. S4) and net surface heat fluxes (Fig. S5) together contributes to about 28% of the total heat budget. It has to be noted that the net surface heat fluxes from different products have large uncertainties (Fig. S5e).

During 2000–2015, prolonged La Niña-like condition and cold phase of PDO shift the convection to the western tropical Pacific resulting in anomalous precipitation and freshening in the western tropical Pacific including the maritime continent. These freshwater anomalies along with the heat are transported to the south Indian Ocean mainly through the

oceanic pathways in the maritime continent and impact the sea level. The enhancement of heat and freshwater intrusion through ITF is discussed in the subsequent section.

3.6 Variability of Indonesian throughflow and south Indian Ocean sea level

The source of heat and freshwater advection and Pacific modulation to the south Indian Ocean sea level is evident from the previous section. Hence, it is very much important to understand the pathway connecting the Pacific to the south Indian Ocean. Studies have documented that the Pacific variability is transported to the south Indian Ocean through ITF which transports fresh and warm Pacific waters to the Indian Ocean (Hu and Sprintall 2016). These fresh and warm water generally spreads westwards by the advection and diffusion within the south equatorial current (Gordon and Fine 1996). According to modern observations and ITF-related modeling studies, the modern ITF is dominated by ENSO variability and climate mean state over the Tropical Pacific (Feng et al. 2017; Mayer et al. 2014; Sprintall et al. 2014). The ITF from the tropical Pacific into the Indian Ocean via the Indonesian seas results in an interocean transport of about 15 Sverdrup and is thought to play an important role in determining the spatial structure of heat and salinity distribution in the Pacific and Indian Oceans (Hu and Sprintall 2016; Lee et al. 2015; Sprintall et al. 2009, 2014). It was also shown that about $36 \pm 7\%$ of the total interannual variability of ITF transport is attributed due to salinity effect.

To understand the ITF variability and its association to the south Indian Ocean sea level, we estimate the Ekman volume transport through Indonesian archipelago as well as thermosteric and halosteric components of ITF transport from ORAS4 and Argo. The Ekman transport is calculated along Nusa Tengarra transect (that is $X_e = 115°$E and $X_w = 131°$E) which capture the flow that exits through Lombok (Lbk), Ombai (Omb), and Timor (Tim) passages into the south Indian Ocean. The transport through major passages like Lombok, Ombai, and Timor contribute to the ITF. The time-series of Ekman volume transport estimated using Eq. (3) from multiple datasets (ERA-interim, Tropflux, and Quickscat) show, an increased southward transport (negative values) since 2000 (Fig. 7a) indicating an increased in the volume transport through ITF.

On annual and longer time scales, the ITF is driven by the large-scale pressure difference between the Pacific and Indian Ocean basins (Wyrtki 1987) and by the enhanced easterlies over the western Pacific. The spatial trend in sea-level pressure anomalies shows increased pressure gradient between the western Pacific and southern Indian Ocean (Fig. S6a). Similarly, the time evolution of sea-level pressure anomaly between western Pacific (140°E–160°E, 5°S–5°N) and south Indian Ocean
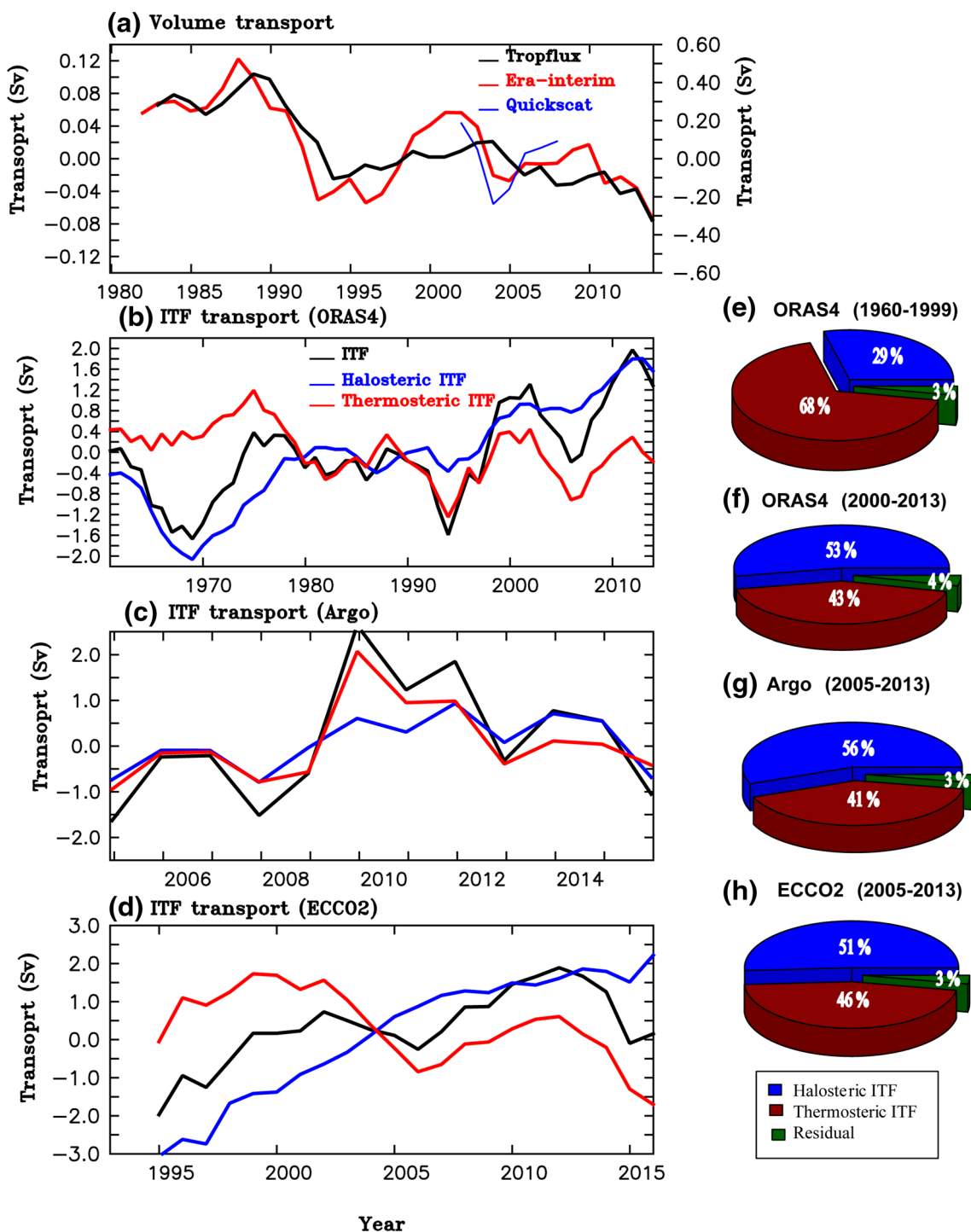
Fig. 7 Time series of annual mean **a** Ekma voluem transport (1SV = 10^{-6}) computed from different wind product along the Indonesian archipelago (115°E–131°E, 6.12°S–7.875°S). Total ITF (black curve), thermosteric component of ITF (ITF$_T$, red curve) and halosteric component of ITF (ITF$_S$, blue curve) from **b** ORAS4, **c** Argo and **d** SODA. The percentage contribution of various contribution to ITF from **e** ORAS4 (1960–1999), **f** ORAS4 (2000–2013), and **g** Argo (2005–2013), **h** ECCO2 (2000–2013)

(80°E–115°E, 20°S–30°S) also show an enhancement of the pressure gradient (Fig. S6b; red curve) indicating an enhancement of ITF transport. The strengthening of anomalous equatorial Pacific easterlies (blue curve; Fig.

S6b) can also be seen during 2000–2015. Strengthened easterly trade winds associated with the co-occurrence of the cold phase of PDO and La Niña-like events resulted

in an anomalously strong Pacific–Indian Ocean pressure gradient, contributing to an increase in ITF.

Further to elaborate the Pacific heat and salinity contributions to the south Indian Ocean sea level through enhanced ITF transport, we estimate the thermosteric (ITF_T) and halosteric (ITF_S) components as well as total ITF transport using Eq. (4) following the approach of Hu and Sprintall (2016). The ITF transport estimated based on density criteria (Fig. 7b; black curve) firmly mimics the Ekman volume flux along the transect of the Indonesian archipelago from ORAS4 as well as Argo data. We have additionally used a high resolution (1/12°) ECCO2 data for

better assessment of ITF variability. The sign of the transport such that positive values indicate transport into the south Indian Ocean (Fig. 7b–d). Increasing ITF transport along with enhanced halosteric contribution (blue curve) can be clearly seen in all the three datasets (Fig. 7b–d). Additionally, we have estimated the percentage contribution of thermosteric and halosteric components of ITF to total ITF by estimating the percentage of absolute values (P_i) of ITF_T and ITF_S relative to the total variation based on Eq. (5) from ORAS4 (Fig. 7e, f), Argo (Fig. 7g), and ECCO2 (Fig. 7h) data. A good agreement between the ITF_T and ITF_S from Argo, ECCO2, and ORAS4 can be
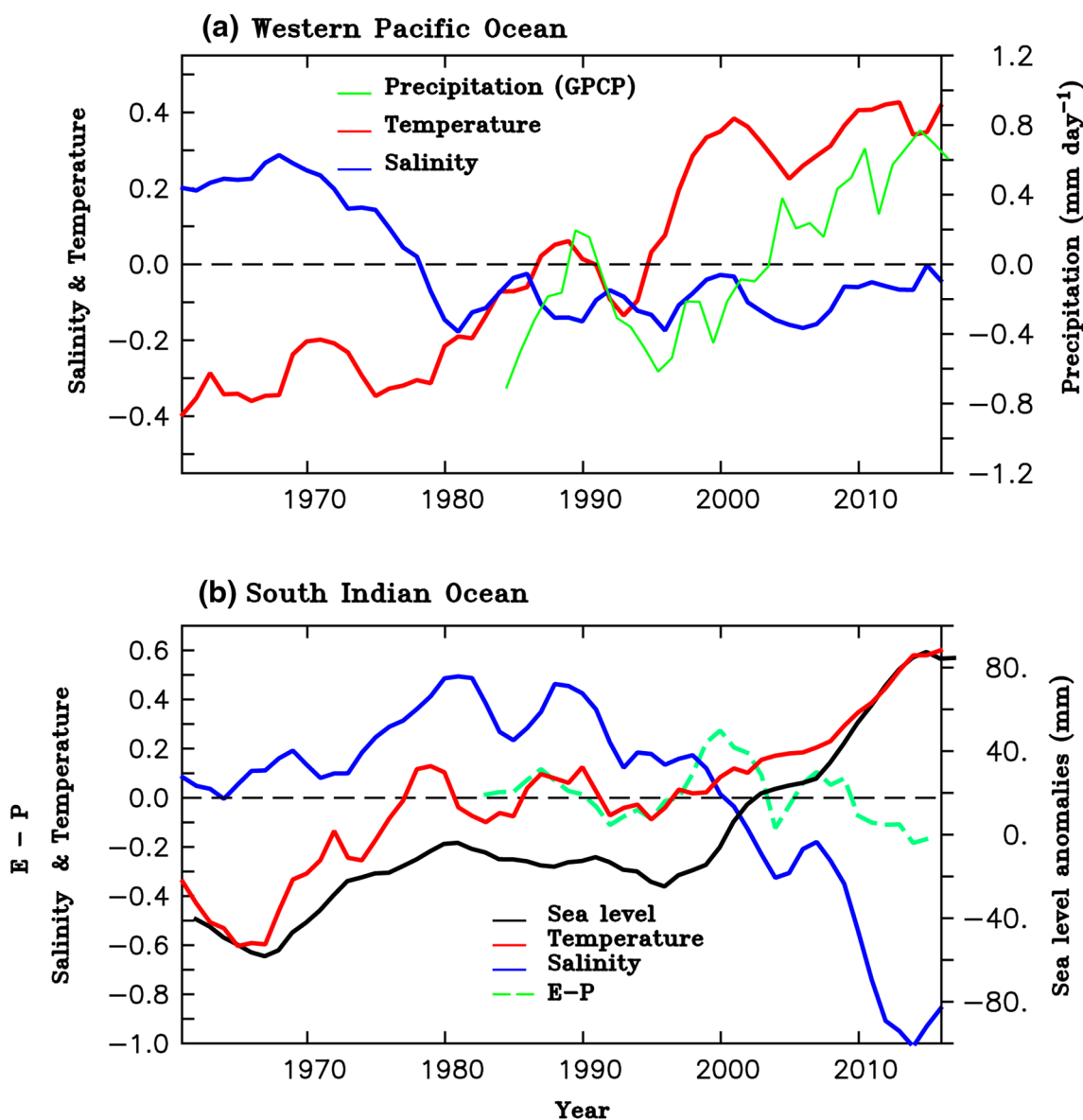

Fig. 8 Time series of annual mean **a** temperature (red curve, °C), salinity (blue curve, PSU) and precipitation (green curve, mm day⁻¹) in the western Pacific, and **b** temperature (red curve, °C), salin-ity (blue curve, PSU), sea level (black curve, mm) and E − P (green curve, m) in the south Indian Ocean (50°E–110°E, 20°S–30°S). The E − P curve is scaled by a factor 2 and shown in **b**

seen from Fig. 7e–h. The ITF$_S$ from Argo, ECCO2, and ORAS4 are 56%, 51%, and 53%, respectively and ITF$_T$ is 41%, 46%, and 43%, respectively. Interestingly, the percentage contribution of ITF is dominated by the halosteric component than the thermosteric component in all the three products. The halosteric contribution to ITF has increased to 53% as compared to 29% during the previous period (1960–1999) in ORAS4. This confirms that the sea-level rise in the south Indian Ocean in recent decades is indeed dominated by the freshwater intrusion from the Pacific freshwater intrusion through ITF has increased during 2000–2015 and this along with enhanced ITF has resulted in the sea-level rise in the south Indian Ocean.

As a result of enhanced ITF, the south Indian Ocean temperature and sea-level show an increase while salinity shows a decrease since 2000 (Fig. 8b). While annual mean freshwater forcing from local contribution (E − P) does not show a significant trend indicating that the contribution from local air-sea fluxes is secondary (Fig. 8b; green dash curve). Concomitantly, anomalous freshening in the western tropical Pacific with an increase in precipitation and a decrease

in salinity can be seen in Fig. 8a. The high salinity is seen in the western Pacific before 1980s gradually decreases as precipitation increase over the western tropical Pacific. The increase in precipitation may be one of the factors contributing to freshening in the western Pacific since the 1980s. The anomalously fresher water from the western tropical Pacific being transported into the south Indian Ocean through the enhanced ITF transport during 2000–2013, which contributes significantly to the halosteric sea-level rise in the south Indian Ocean.

In summary, sea-level rise in the southern Indian Ocean has accelerated due to enhanced halosteric sea-level rise modulated by Pacific variability. The stronger in-phase association of major Pacific climate modes, PDO and La Niña-like condition enhances the equatorial Pacific easterly winds which in-turn enhances the ITF and transport anomalously fresh and warm water from the western tropical Pacific into the south Indian Ocean. As a result, south Indian Ocean sea-level rise has accelerated more than the global, with 40% contribution from the halosteric sea level primarily through

Fig. 9 The time series of annual mean **a** sea-level anomalies from ORAS4 in the south Indian Ocean (red curve; mm), PDO index (blue curve) from observation; **b** mean sea-level anomalies (red curve, mm), PDO index (blue curve) from the proxy records
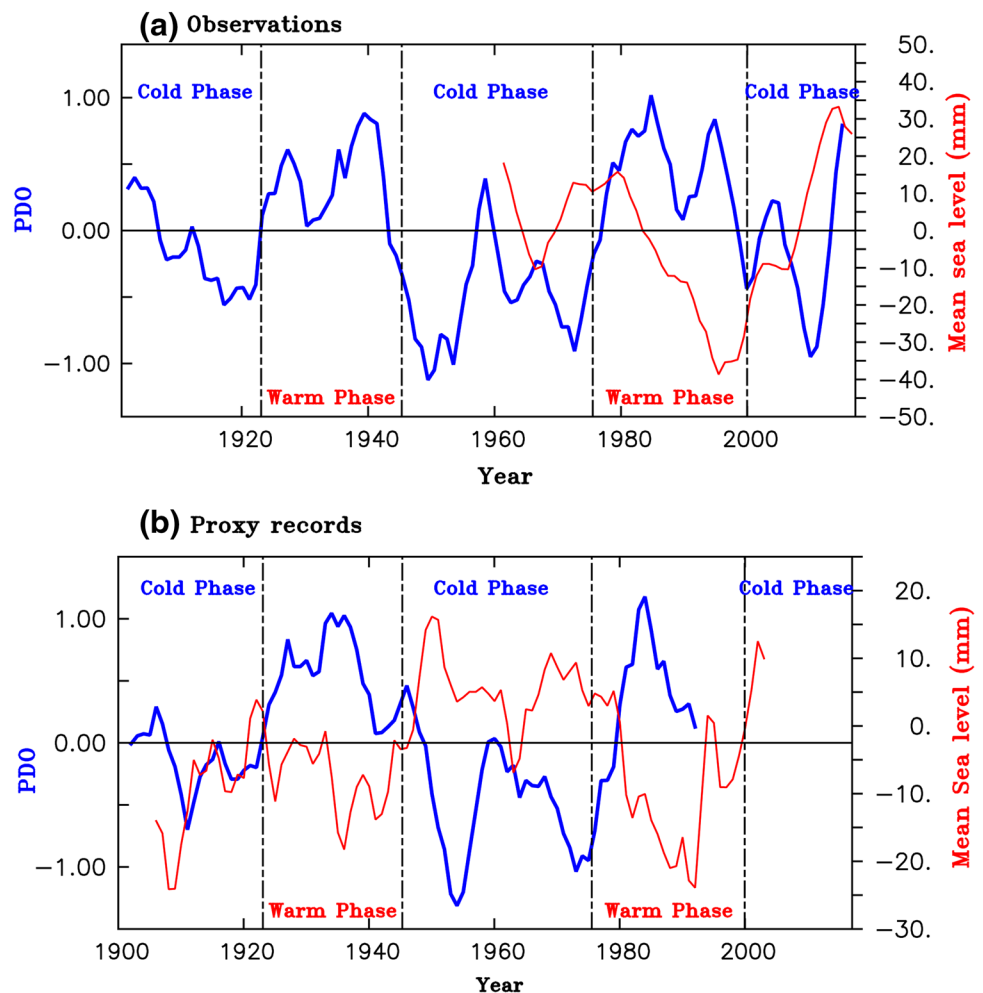
the ITF transport and a secondary contribution from the local processes during 2000–2015.

4 Evidence from long-term proxy records to the south Indian Ocean sea-level variability

We have seen that the south Indian Ocean sea-level variations are closely associated with the phases of PDO and ENSO. Therefore, it will be interesting to know whether such variability is a part of the internal mode of variability modulated on the multi-decadal timescale. To achieve this, we present a long-term proxy record of sea-level and PDO reconstruction (details are in Sect. 2). These proxy records are used to support our finding that sea-level rise in the south Indian Ocean has co-evolved with the cold phases of PDO is also evident from the long-term proxy records. Enhanced freshwater contribution to the south Indian Ocean sea level is seen only during the recent cold PDO phase and there are no proxy salinity records available during the recent decades to support the influence of salinity on the south Indian Ocean sea-level rise.

Time evolution of long-term proxy record of PDO matches well with the observed time series, especially in capturing the cold and warm phases of PDO (Fig. 9a, b; blue curve). Long-term proxy sea-level anomalies (Fig. 9b; red curve) from the south-eastern Indian Ocean reveals a good association with PDO phases with high sea level in the south Indian Ocean during cold PDO phases and vice versa. These indicate that the association between the PDO and south Indian Ocean sea level is seen over a period of time. Further, to confirm the co-evolution, we have performed a cross-spectral analysis of the south Indian Ocean proxy sea level with the PDO (Fig. 10). The significance at a 90% (blue curve) and 95% confidence level (red curve) is shown for the variance spectra. The time interval used for a cross-spectral analysis between the south Indian Ocean sea level and PDO index is during 1795–1991. To identify common trends and features related to internal climate variability we compare sea level records from the south Indian Ocean with the PDO index from proxy records. Further, it is found that the south Indian Ocean sea-level records are coherent with the PDO index at a period centered at 12.5–16 years (Fig. 10c). These results reveal that the south Indian Ocean sea-level variability is majorly modulated by the Pacific variability and the association is part of the internal mode of variability modulated on decadal time-scales. The time series and coherence are shown in Fig. 10 are for the overlapping period. Additionally, we have shown the time-series of PDO and sea level for the available period in Fig. S7.

The detailed mechanism of south Indian Ocean sea-level rise is synthesized in the schematic shown in Fig. 11.
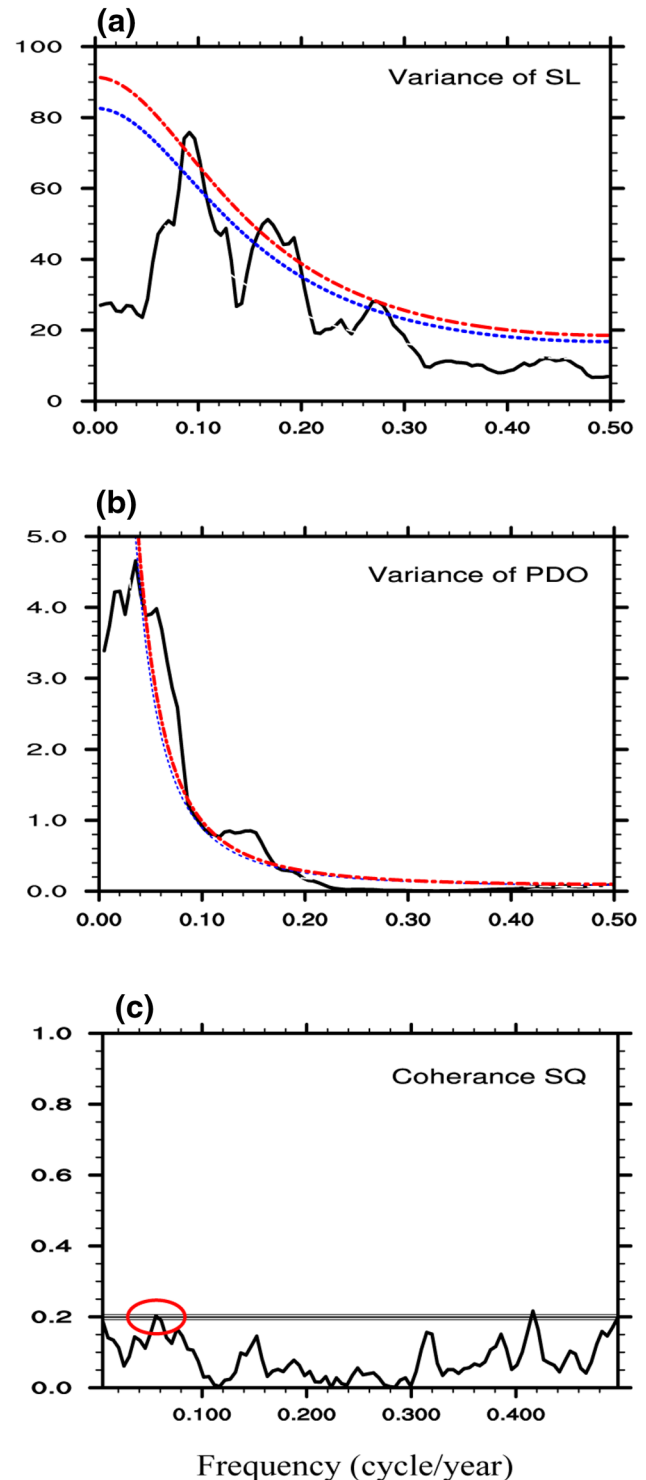

Fig. 10 Variance spectra of the **a** sea level, **b** PDO index and **c** coherence of sea level and PDO. The significance at a 90% (blue curve) and 95% (red curve) confidence level is shown by the dashed line

5 Conclusions and implications

Indian Ocean region is heavily populated, comprises of many low-lying islands and coastal zones, and is highly rich in marine eco-system. Sea level in the Indian Ocean has shown a distinct spatial pattern with an increase in the north (Srinivasu et al. 2017; Swapna et al. 2017; Thompson et al. 2016) and a substantial increase in the south Indian Ocean, south of 20°S (Fig. 1a, b). The south Indian Ocean sea-level rise is about 5.2 mm year^{-1} during 2000–2015, which is 37% quicker than the global mean sea-level rise.
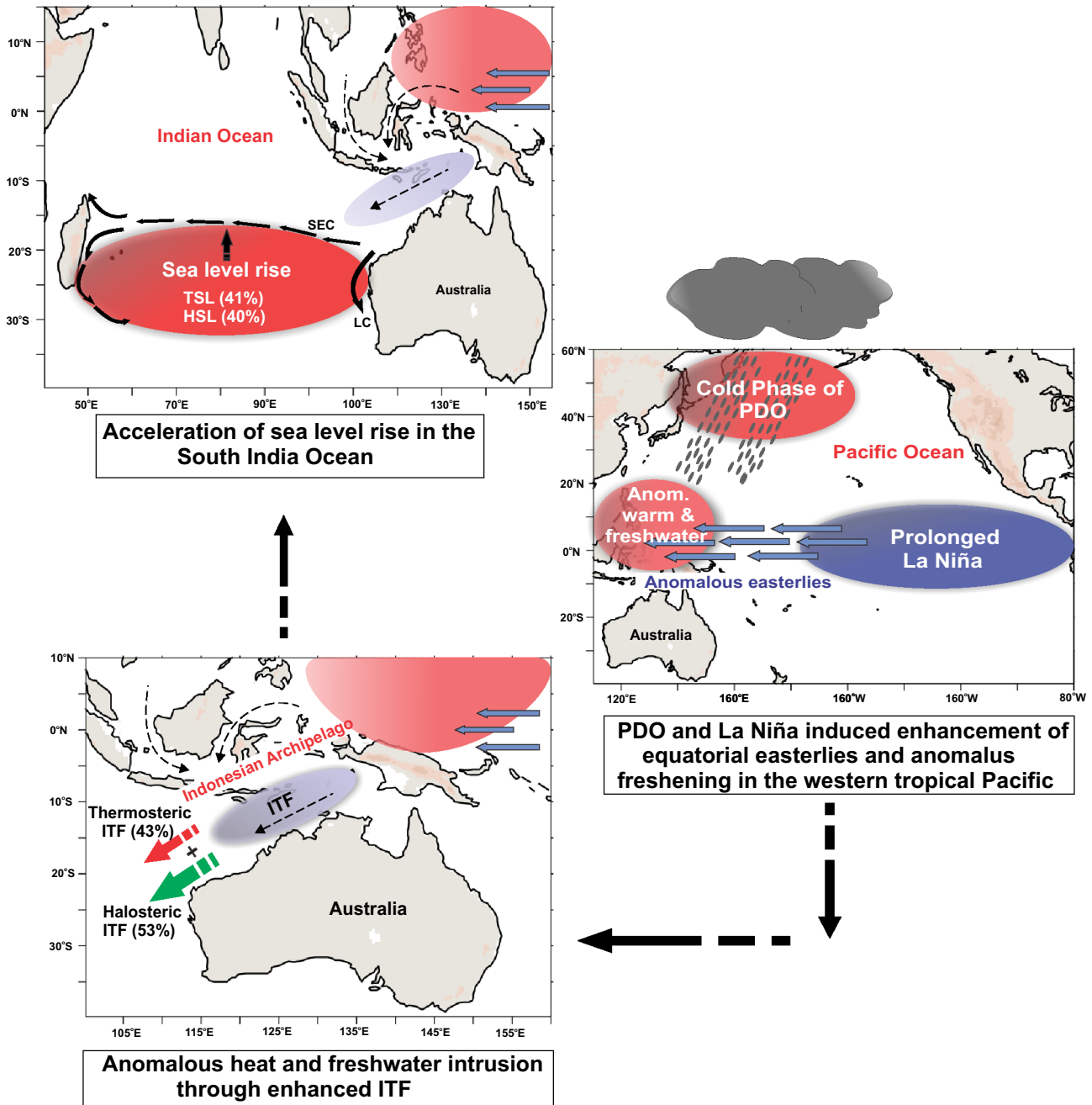
Fig. 11 Schematic diagram showing the mechanism responsible for the accelerated sea-level rise in the south Indian Ocean during the twenty-first century. TSL denotes thermosteric sea level and HSL, halosteric sea level. Indonesian Throughflow is denoted as IFT, and LC and SEC indicate Leeuwin current and south equatorial current

Recent studies have highlighted the intrusion of heat from the western Pacific into the south Indian Ocean resulting in global warming hiatus. The intrusion of heat during warming hiatus has resulted in mass coral bleaching events in the south Indian Ocean (Zinke et al. 2015; Feng et al. 2015a, b). Though the warming hiatus and its implications have been studied extensively, the accelerated sea-level rise in the south Indian Ocean and the contributing mechanism remains unknown.

In the present study, we used long-term tide gauge records, satellite, Argo, and reanalysis datasets to delineate the mechanism and identify contributing terms for the accelerated sea-level rise in the south Indian Ocean. Our results reveal Pacific modulation with enhanced freshwater intrusion from the Pacific through the ITF is the primary contributor to the sea-level rise in the south Indian Ocean. While the role of other processes, such as surface air-sea heat fluxes and local freshwater forcing along with changes in Ekman pumping has a secondary contribution to south Indian Ocean sea-level rise. Prolonged La Niña-like condition and cold phase of PDO enhance the equatorial Pacific easterlies, which in-turn enhances the ITF. Increased ITF transports fresh and warm water from the Pacific into the south Indian Ocean. As a result, the south Indian Ocean sea-level rise has accelerated 37% more than the global, with a 40% contribution from the halosteric sea-level during 2000–2015. The Long-term proxy records reveal internal mode variability in modulating south Indian Ocean sea level. The findings from the study caution possibilities of heat and freshwater intrusion from the Pacific, which may lead to extreme marine heat waves and cause the vulnerability of coral reefs and the marine ecosystem.

References

Adler RF, Huffman GJ, Chang A, Ferraro R, Xie PP, Janowiak J et al (2003) The version-2 global precipitation climatology project (GPCP) monthly precipitation analysis (1979–present). J Hydrometeor 4:1147–1167. https://doi.org/10.1175/1525-7541(2003)004<1147:TVGPCP>2.0.CO;2

Allan R, Ansell T (2006) A new globally complete monthly historical gridded mean sea level pressure dataset (HadSLP2): 1850–2004. J Clim 19:5816–5842. https://doi.org/10.1175/JCLI3937.1

Backeberg BC, Penven P, Rouault M (2012) Impact of intensified Indian Ocean winds on mesoscale variability in the Agulhas system. Nat Clim Change 2:608–612. https://doi.org/10.1038/nclimate1587

Balmaseda MA, Mogensen K, Weaver AT (2013) Evaluation of the ECMWF ocean reanalysis system ORAS4. Q J R Meteorol Soc 139:1132–1161. https://doi.org/10.1002/qj.2063

Berrisford P et al (2009) The ERA-interim archive. ERA report series, no. 1. ECMWF, Reading

Bindoff NL et al (2007) Observations: oceanic climate change and sea level. In: Climate change 2007: the physical science basis. Contribution of working group I to the fourth assessment report of the intergovernmental panel on climate change. Cambridge University Press, Cambridge, UK and New York, NY, USA, pp 385–432

Bjerknes J (1969) Atmospheric teleconnections from the equatorial Pacific. Mon Weather Rev 97:163–172. https://doi.org/10.1175/1520-0493(1969)097<0163:ATFTEP>2.3.CO;2

Chambers DP, Cazenave A, Champollion N (2017) Evaluation of the global mean sea level budget between 1993 and 2014. Surv Geophys 38:309. https://doi.org/10.1007/s10712-016-9381-3

Chen X, Zhang X, Church JA, Watson CS, King MA, Monselesan D, Legresy B, Harig C (2017) The increasing rate of global mean sea-level rise during 1993–2014. Nat Clim Change 7:7–492. https://doi.org/10.1038/Nclimate3325

Church JA, White NJ (2011) Sea-level rise from the late 19th to the early 21st century. Surv Geophys 32:585–602. https://doi.org/10.1007/s10712-011-9119-1

Dangendorf S, Rybski D, Mudersbach C et al (2014) Evidence for long-term memory in sea level. Geophys Res Lett 41:5530–5537. https://doi.org/10.1002/2014gl060538

De Ruijter W (1982) Asymptotic analysis of the Agulhas and Brazil current systems. J Phys Oceanogr 12:361–373. https://doi.org/10.1175/1520-0485(1982)012<0361:aaotaa>2.0.co;2

Dieng HB, Cazenave A, Meyssignac B, Ablain M (2017) New estimate of the current rate of sea level rise from a sea level budget approach. Geophys Res Lett 44:3744–3751. https://doi.org/10.1002/2017gl073308

Dong L, McPhaden MJ (2016) Interhemispheric SST gradient trends in the Indian Ocean prior to and during the recent global warming hiatus. J Clim 29:9077–9095. https://doi.org/10.1175/jcli-d-16-0130.1

Dong L, Zhou T (2013) Steric sea level change in twentieth-century historical climate simulation and IPCC-RCP8.5 scenario projection: a comparison of two versions of FGOALS model. Adv Atmos Sci 30:841. https://doi.org/10.1007/s00376-012-2224-3

Du Y et al (2015) Decadal trends of the upper ocean salinity in the tropical Indo-Pacific since mid-1990s. Sci Rep 5:16050. https://doi.org/10.1038/srep16050

Ducet N, Le Traon PY, Reverdin G (2000) Global high-resolution mapping of ocean circulation from TOPEX/Poseidon and ERS-1 and -2. J Geophys Res Oceans 105(C8):19477–19498

England MH, Mcgregor S, Spence P et al (2014) Recent intensification of wind-driven circulation in the Pacific and the ongoing warming hiatus. Nat Clim Change 4:222–227. https://doi.org/10.1038/nclimate2106

Felis T, Suzuki A, Kuhnert H et al (2010) Pacific decadal oscillation documented in a coral record of North Pacific winter temperature since 1873. Geophys Res Lett 37:2000–2005. https://doi.org/10.1029/2010gl043572

Feng M, Böning C, Biastoch A et al (2011) The reversal of the multidecadal trends of the equatorial Pacific easterly winds, and the Indonesian throughflow and Leeuwin current transports. Geophys Res Lett 38:1–6. https://doi.org/10.1029/2011gl047291

Feng M, Hendon HH, Xie S-P, Marshall AG, Schiller A, Kosaka Y, Caputi N, Pearce A (2015a) Decadal increase in Ningaloo Niño since the late 1990s. Geophys Res Lett 42:104–112. https://doi.org/10.1002/2014gl062509

Feng M, Benthuysen M, Zhang N, Slawinski D (2015b) Freshening anomalies in the Indonesian throughflow and impacts on the

Leeuwin current during 2010–2011. Geophys Res Lett 42:8555–8562. https://doi.org/10.1002/2015gl065848

Feng M, Zhang X, Sloyan B, Chamberlain M (2017) Contribution of the deep ocean to the centennial changes of the Indonesian throughflow. Geophys Res Lett 44:2859–2867. https://doi.org/10.1002/2017gl072577

Fore AB, Stiles A, Chau B, Williams R, Dunbar Rodrıguez E (2014) Point-wise wind retrieval and ambiguity removal improvements for the QuikSCAT climatological data set. IEEE Trans Geosci Remote Sens 99:1–9. https://doi.org/10.1109/TGRS.2012.2235843

Gershunov A, Barnett TP (1998) interdecadal modulation of enso teleconnections. Bull Am Meteorol Soc 79:2715–2726. https://doi.org/10.1175/1520-0477(1998)079<2715:IMOET>2.0.CO;2

Good SA, Martin MJ, Rayner NA (2013) EN4: quality controlled ocean temperature and salinity profiles and monthly objective analyses with uncertainty estimates. J Geophys Res Ocean 118:6704–6716. https://doi.org/10.1002/2013jc009067

Gordon AL, Fine RA (1996) Pathways of water between the Pacific and Indian Oceans in the Indonesians seas. Nature 379:146–149

Gordon AL, Sprintall J, Van Aken HM et al (2010) The Indonesian throughflow during 2004–2006 as observed by the INSTANT program. Dyn Atmos Ocean 50:115–128. https://doi.org/10.1016/j.dynatmoce.2009.12.002

Han W, Meehl GA, Balaji R, Fasullo JT, Hu A, Lin J et al (2010) Patterns of Indian Ocean sea-level change in a warming climate. Nat Geosci 3(8):546–550. https://doi.org/10.1038/ngeo901

Han W, Vialard J, McPhaden MJ et al (2014) Indian Ocean decadal variability: a review. Bull Am Meteorol Soc 95:1679–1703. https://doi.org/10.1175/bams-d-13-00028.1

Hosoda S, Ohira T, Nakamura T (2008) A monthly mean dataset of global oceanic temperature and salinity derived from Argo floats observations. JAMSTEC 8:47–59

Hu S, Sprintall J (2016) Interannual variability of the Indonesian throughflow: the salinity effect. J Geophys Res Oceans 121:2596–2615. https://doi.org/10.1002/2015jc011495

Hu S, Sprintall J (2017) observed strengthening of interbasin exchange via the Indonesian seas due to rainfall intensification. Geophys Res Lett 44:1448–1456. https://doi.org/10.1002/2016gl072494

Ishii M, Fukuda Y, Hirahara S et al (2017) Accuracy of global upper ocean heat content estimation expected from present observational data sets. Sola 13:163–167. https://doi.org/10.2151/sola.2017-030

Jadhav J, Panickal S, Marathe S, Ashok K (2015) On the possible cause of distinct El Niño types in the recent decades. Sci Rep. https://doi.org/10.1038/srep17009

Kendall MG (1975) Rank correlation methods, 4th edn. Charles Griffin, London

Kistler R, Kalnay E, Collins W, Saha S, White G, Woollen J et al (2001) The NCEP–NCAR 50-year reanalysis: monthly means CD-ROM and documentation. Bull Am Meteorol Soc 82:247–268. https://doi.org/10.1175/1520-0477(2001)082<0247:TNNYRM>2.3.CO;2

Kumar BP, Vialard J, Lengaigne M et al (2012) TropFlux: air-sea fluxes for the global tropical oceans-description and evaluation. Clim Dyn 38:1521–1543. https://doi.org/10.1007/s00382-011-1115-0

Landerer FW, Jungclaus JH, Marotzke J (2007) Regional dynamic and steric sea level change in response to the IPCC-A1B scenario. J Phys Oceanogr 37:296–312. https://doi.org/10.1175/JPO3013.1

Lee T, McPhaden MJ (2008) Decadal phase change in large-scale sea level and winds in the Indo-Pacific region at the end of the 20th century. Geophys Res Lett 35:L01605. https://doi.org/10.1029/2007GL032419

Lee SK, Park W, Baringer MO et al (2015) Pacific origin of the abrupt increase in Indian Ocean heat content during the warming hiatus. Nat Geosci 8:445–449. https://doi.org/10.1038/ngeo2438

Legeais JF, Ablain M, Zawadzki L et al (2018) An improved and homogeneous altimeter sea level record from the ESA climate change initiative. Earth Syst Sci Data 10:281–301. https://doi.org/10.5194/essd-10-281-2018

Levitus S, Antonov JI, Boyer TP et al (2012) World ocean heat content and thermosteric sea level change (0–2000 m), 1955–2010. Geophys Res Lett 39:1–5. https://doi.org/10.1029/2012gl051106

Li Y, Han W (2015) Decadal sea level variations in the Indian Ocean investigated with HYCOM: roles of climate modes, ocean internal variability, and stochastic wind forcing. J Clim 28:9143–9165. https://doi.org/10.1175/JCLI-D-15-0252.1

Li Y, Han W, Zhang L (2017) Enhanced decadal warming of the southeast Indian Ocean during the recent global surface warming slowdown. Geophys Res Lett. https://doi.org/10.1002/2017gl075050

Li Y, Han W, Hu A, Meehl GA, Wang F (2018) Multidecadal changes of the upper Indian Ocean heat content during 1965–2016. J Clim 31:7863–7884. https://doi.org/10.1175/JCLI-D-18-0116.1

Liu W, Shang-Ping X, Jian L (2016) Tracking ocean heat uptake during the surface warming hiatus. Nat Commun 7:10926. https://doi.org/10.1038/ncomms10926

Llovel W, Lee T (2015) Importance and origin of halosteric contribution to sea level change in the southeast Indian Ocean during 2005–2013. Geophys Res Lett 42:1148–1157. https://doi.org/10.1002/2014GL062611

Mann HB (1945) Nonparametric test against trend. Econometrica 13:245–259

Mantua NJ, Hare SR, Zhang Y et al (1997) A Pacific interdecadal climate oscillation with impacts on salmon production. Bull Am Meteorol Soc 78:1069–1080. https://doi.org/10.1175/1520-0477(1997)078<1069:APICOW>2.0.CO;2

Mayer M, Haimberger L, Balmaseda MA (2014) On the energy exchange between tropical ocean basins related to ENSO. J Clim 27:6393–6403. https://doi.org/10.1175/jcli-d-14-00123.1

Meehl GA, Arblaster JM, Fasullo JT et al (2011) Model-based evidence of deep-ocean heat uptake during surface-temperature hiatus periods. Nat Clim Change 1:360–364. https://doi.org/10.1038/nclimate1229

Menemenlis D, Campin J, Heimbach P, Hill C et al (2008) ECCO2: high-resolution global ocean and sea ice data synthesis. AGU fall meeting abstracts OS31C-1292

Narayanasetti S, Swapna P, Ashok K, Jadhav J, Krishnan R (2016) Changes in biological productivity associated with NingalooNiño/Niña events in the southern subtropical Indian Ocean in recent decades. Sci Rep. https://doi.org/10.1038/srep27467

Neelin JD, Battisti DS, Hirst AC, Jin F-F, Wakata Y, Yamagata T, Zebiak SE (1998) ENSO theory. J Geophys Res 103(C7):14261–14290. https://doi.org/10.1029/97JC03424

Nerem RS, Beckley BD, Fasullo J, Hamlington BD, Masters D, Mitchum GT (2018) Climate change-driven accelerated sea level rise detected in the Altimeter era. Proc Natl Acad Sci USA 115:2022–2025. https://doi.org/10.1073/pnas.1717312115

Nidheesh AG, Lengaigne M, Vialard J et al (2013) Decadal and long-term sea level variability in the tropical Indo-Pacific Ocean. Clim Dyn 41:381–402. https://doi.org/10.1007/s00382-012-1463-4

Nidheesh AG, Lengaigne M, Vialard J et al (2017) Robustness of observation-based decadal sea level variability in the Indo-Pacific Ocean. Geophys Res Lett 44:7391–7400. https://doi.org/10.1002/2017gl073955

Nieves VJ, Willis K, Patzert WC (2015) Recent hiatus caused by decadal shift in Indo-Pacific heating. Science 349:532–535. https://doi.org/10.1126/science.aaa4521

Oliver ECJ et al (2018) Longer and more frequent marine heatwaves over the past century. Nat Commun. https://doi.org/10.1038/s41467-018-03732-9

Qu T, Du Y, Meyers G, Ishida A, Wang D (2005) Connecting the tropical Pacific with Indian Ocean through South China Sea. Geophys Res Lett 32:L24609. https://doi.org/10.1029/2005GL024698

Qu T, Fukumori I, Fine RA (2019) Spin-up of the Southern Hemisphere super gyre. J Geophys Res Oceans 124:154–170. https://doi.org/10.1029/2018JC014391

Rhein M et al (2013) Chapter 3; observations: ocean, fifth assessment report intergovernmental. Panel climate change

Rietbroek R, Brunnabend S-E, Kusche J et al (2016) Revisiting the contemporary sea-level budget on global and regional scales. Proc Natl Acad Sci 113:1504–1509. https://doi.org/10.1073/pnas.1519132113

Schwarzkopf FU, Boning CW (2011) Contribution of Pacific wind stress to multi-decadal variations in upper-ocean heat content and sea level in the tropical south Indian Ocean. Geophys Res Lett 38:1–6. https://doi.org/10.1029/2011gl047651

Sprintall J, Liu T (2005) Ekman mass and heat transport in the Indonesia Seas. Oceanography 18:88–97. https://doi.org/10.5670/oceanog.2005.09

Sprintall J, Wijffels SE, Molcard R, Jaya I (2009) Direct estimates of the Indonesian throughflow entering the Indian ocean: 2004-2006. J Geophys Res Ocean 114:2004–2006. https://doi.org/10.1029/2008jc005257

Sprintall J, Gordon AL, Koch-Larrouy A et al (2014) The Indonesian seas and their role in the coupled ocean-climate system. Nat Geosci 7:487–492. https://doi.org/10.1038/ngeo2188

Srinivasu U, Ravichandran M, Han W, Rahman H, Yuanlong L, Shailesh N (2017) Causes for the reversal of north Indian Ocean decadal sea level trend in recent two decades. Clim Dyn 49:3887. https://doi.org/10.1007/s00382-017-3551-y

Swapna P, Jyoti J, Krishnan R, Sandeep N, Griffies SM (2017) Multidecadal weakening of Indian summer monsoon circulation induces an increasing northern Indian Ocean sea level. Geophys Res Lett 44:10-560. https://doi.org/10.1002/2017GL074706

Thompson PR, Piecuch CG, Merrifield MA, McCreary JP, Firing E (2016) Forcing of recent decadal variability in the equatorial and north Indian Ocean. J Geophys Res Oceans 121:6762–6778. https://doi.org/10.1002/2016jc012132

Trenary LL, Han W (2013) Local and remote forcing of decadal sea level and thermocline depth variability in the south Indian Ocean. J Geophys Res Ocean 118:381–398. https://doi.org/10.1029/2012jc008317

Wijffels S, Mayer G (2004) An intersection of oceanic waveguides: variability in the Indonesian throughflow region. J Phys Oceanogr 34:1232–1253 .https://doi.org/10.1175/1520-0485(2004)034<1232:AIOOWV>2.0.CO;2

Woodworth PL, Player R (2003) The permanent service for mean sea level: an update to the 21st century. J Coast Res 19:287–295

Wyrtki K (1987) Indonesian through flow and the associated pressure gradient. J Geophys Res 92(C12):12941–12946. https://doi.org/10.1029/JC092iC12p12941

WCRP Global Sea Level Budget Group (2018) Global sea-level budget 1993–present. Earth System Science Data 10:1551–1590. https://doi.org/10.5194/essd-10-1551-2018

Yu L, Jin X, Weller RA (2008) Multidecade global flux datasets from the objectively analyzed air-sea fluxes (OAFlux) project: latent and sensible heat fluxes, ocean evaporation, and related surface meteorological variables. Woods Hole Oceanographic Institution, OAFlux project technical report. OA-2008-01, 64. Woods Hole, MA

Zhang Y, Feng M, Du Y, Phillips HE, Bindoff NL, McPhaden MJ (2018) Strengthened Indonesian throughflow drives decadal warming in the Southern Indian Ocean. Geophys Res Lett 45:6167–6175. https://doi.org/10.1029/2018GL078265

Zhou L, Murtugudde R, Jochum M (2008) Dynamics of the intraseasonal oscillations in the Indian Ocean South. J Clim 1:121–132. https://doi.org/10.1175/2007jpo3730.1

Zinke J, Hoell A, Lough JM et al (2015) Coral record of southeast Indian Ocean marine heatwaves with intensified Western Pacific temperature gradient. Nat Commun 6:1–9. https://doi.org/10.1038/ncomms9562